

## NEAR-IR PROPERTIES OF GALAXY CLUSTERS: LUMINOSITY AS A BINDING MASS PREDICTOR AND THE STATE OF CLUSTER BARYONS

YEN-TING LIN<sup>1</sup>, JOSEPH J. MOHR<sup>1,2</sup> AND S. A. STANFORD<sup>3,4</sup>

*Submitted to ApJ December 6, 2002, Accepted March 25, 2003*

### ABSTRACT

We explore the near-infrared properties of galaxies within 27 galaxy clusters using data from the Two Micron All Sky Survey (2MASS). For a subsample of 13 clusters with available X-ray imaging data, we examine both the properties of the galaxies and the intracluster medium. We show that the  $K$ -band luminosity is correlated with cluster mass, providing a binding mass estimate accurate to 45%. The mass-to-light ratio in our ensemble increases by a factor of  $\sim 2$  over the cluster mass range ( $10^{14}M_{\odot} - 10^{15}M_{\odot}$ ). We examine the total baryon fraction, showing that it is an increasing function of cluster mass. Using the mass-to-light ratio of massive clusters, we find that  $\Omega_M = 0.19 \pm 0.03$ ; using the total baryon fraction we find that  $\Omega_M = 0.28 \pm 0.03$ , in good agreement with recent cosmic microwave background (CMB) anisotropy constraints. Differences between these two estimates suggest that the  $K$ -band mass-to-light ratio in massive clusters may be lower than that in the universe by as much as  $\sim 30\%$ .

We examine the stellar mass fraction, the intracluster medium (ICM) mass to stellar mass ratio and the cluster iron mass fraction. The stellar mass fraction decreases by a factor of 1.8 from low to high mass clusters, and the ICM to stellar mass ratio increases from 5.9 to 10.4 over the same mass range. Together, these measurements suggest a decrease of star formation efficiency with increasing cluster mass and provide constraints on models of the thermodynamic history of the intracluster medium. The cluster iron mass to total mass ratio is constant and high, suggesting that some efficient, and uniform enrichment process may have taken place before the bulk of stars in cluster galaxies formed.

*Subject headings:* cosmology: observation – galaxies: clusters, luminosity function – infrared: galaxies

### 1. INTRODUCTION

Galaxy clusters are central to many cosmological studies. The local cluster abundance is a direct measure of the present-day matter power spectrum amplitude and the dark matter density (White et al. 1993a; Viana & Liddle 1999; Reiprich & Böhringer 2002). The cluster redshift distribution constrains the growth of density perturbations, and this effect can be used to constrain the amount and nature of the dark matter and dark energy (Wang & Steinhardt 1998; Haiman et al. 2001; Holder et al. 2001; Levine et al. 2002; Majumdar & Mohr 2002). The baryon fraction of the most massive local galaxy clusters has been used to constrain the matter density parameter (White et al. 1993b; David et al. 1995; White & Fabian 1995; Mohr et al. 1999; Grego et al. 2001), and the spatial distribution of galaxy clusters has been used to measure the power spectrum of density perturbations (Bahcall & Soneira 1983; Miller & Batuski 2001; Schuecker et al. 2002).

The galaxy cluster halo mass is crucial to the interpretation of each of the cosmological measurements mentioned above. The cluster halo mass, which is dominated by dark matter, is not a direct observable; a good mass indicator is required to bridge the gap between the observational and theoretical realms. Detailed mass estimators relying on hydrostatic or virial equilibrium or on the weak lensing distortions of background galaxies have been developed, but

generally these estimates require extensive X-ray and optical imaging and/or spectroscopy. The large cluster surveys that are being planned and carried out to measure the cluster redshift and spatial distribution will produce large samples dominated by systems that are near the detection threshold. Deep follow up of each of these systems with an X-ray telescope or multiobject spectrograph is implausible, and so the analyses of these future surveys will rely on the existence of simpler and perhaps less accurate mass estimators. Specifically, these surveys will employ scaling relations between simple cluster observables like the X-ray luminosity or the Sunyaev-Zel'dovich effect (SZE; Sunyaev & Zel'dovich 1970, 1972) luminosity and cluster halo mass.

Observations over the past several years have demonstrated that clusters exhibit significant regularity (Mohr & Evrard 1997; Arnaud & Evrard 1999; Mohr et al. 1999), and we now have several locally calibrated mass-observable relations. Among these are the mass-X-ray temperature relation ( $M - T_X$ , e.g. Finoguenov et al. 2001b), the mass-luminosity relation ( $M - L_X$ , e.g. Reiprich & Böhringer 2002) and the mass-velocity dispersion relation ( $M - \sigma_V$ , e.g. Girardi et al. 2000). Here we use the Two Micron All Sky Survey (2MASS) to explore whether the galaxy light itself is a good indicator of the cluster mass by examining the cluster halo mass- $K$ -band light relation. Such a relation would be extremely valuable for interpreting any cluster survey with near-IR (hereafter

<sup>1</sup>Department of Astronomy, University of Illinois, Urbana, IL 61801; ylin2@astro.uiuc.edu

<sup>2</sup>Department of Physics, University of Illinois, Urbana, IL 61801; jmohr@uiuc.edu

<sup>3</sup>Physics Department, University of California at Davis, Davis, CA 95616; adam@igpp.uclnl.org

<sup>4</sup>Institute of Geophysics and Planetary Physics, Lawrence Livermore National Laboratory, Livermore, CA 94551

NIR) coverage.

In addition to the cosmological studies, there is a range of unresolved questions surrounding the star formation history of the universe, and the thermodynamic history of the intergalactic and intracluster medium (hereafter ICM). The galaxy NIR light in combination with X-ray imaging and spectroscopy are well suited to address these issues, because the X-ray observations provide measures of the halo and ICM masses and the NIR light appears to be a good tracer of the total stellar mass. The effects of dust in NIR wavebands are rather small compared to optical and ultraviolet (UV) wavebands. The NIR light is less sensitive to the recent star formation history in galaxies. Studies of a large sample of spiral galaxies (Gavazzi et al. 1996) indicate that the  $H$ -band luminosity is proportional to the galaxy dynamical mass, implying that  $H$ -band light can serve as a better mass estimator than  $U$ ,  $B$  or  $V$ -band light. Modeling suggests that the  $K$ -band mass-to-light ratio can still vary by as much as a factor of two over a range of galaxy Hubble type, color, and star formation histories (Madau et al. 1998; Pahre et al. 1998), so care must be taken to account for these variations wherever possible.

Massive galaxy clusters largely exhibit self-similar scaling relations, but that behavior does not hold for less massive clusters and groups (e.g. Lloyd-Davies et al. 2000; Voit et al. 2002). Non-gravitational processes, such as feedback due to star formation activity in galaxies or AGN heating may significantly alter the structure of the lower mass systems, but important questions remain about which processes are important. By studying the state of the baryons in present epoch clusters, one can in principle unravel details of their formation and evolution. For example, the distribution of the ICM gas may give clues to the importance of non-gravitational heating (Cavaliere et al. 1997; Mohr et al. 1999; Bialek et al. 2001); the total stellar content within a cluster measures the cooled baryon fraction, which in turn describes the efficiency of galaxy formation in the clusters (Bryan 2000); the metallicity of the ICM gas also provides stringent constraints on the star formation history of cluster galaxies, as well as on the mechanisms that transport the metals from the galaxies into the ICM (Arnaud et al. 1992; Renzini 1997). Among the 27 clusters in our sample, we have measured the ICM mass for a subsample of 13 systems. This, together with the total stellar mass inferred from the NIR luminosity, gives us an opportunity to address different preheating, star formation and enrichment scenarios.

This paper is structured as follows. In §2 we describe how we infer the cluster virial mass from X-ray temperature, how the total NIR galaxy luminosity is obtained from the 2MASS data, and how the ICM mass is measured using X-ray data. We present the NIR mass-luminosity relation, as well as the mass-to-light ratio for our sample of clusters in §3. In the rest of §3 we examine constraints on the density parameter  $\Omega_M$  using the cluster mass-to-light ratio (§3.1) and the total baryon fraction (§3.2). We compare the results and discuss the cosmological implications in §3.3. In §4 we examine the cluster baryon reservoirs in more detail. The discussion includes the star formation efficiency on cluster mass scales (§4.1), the relative distribution of baryons in the ICM and in galaxies (§4.2),

and the ICM iron abundance and clues on the enrichment (§4.3). Finally, we present our conclusions, discuss the robustness of our analysis, the possible systematics, and prospects for further investigation in §5 & §6.

Throughout the paper we assume the density parameters for the matter and the cosmological constant to be  $\Omega_M = 0.3$ ,  $\Omega_\Lambda = 0.7$ , respectively, and the Hubble parameter to be  $H_0 = 70 h_{70} \text{ km s}^{-1} \text{ Mpc}^{-1}$ .

## 2. JOINT NIR AND X-RAY ANALYSIS

We use the observed X-ray mass-temperature relation together with published X-ray emission weighted mean temperatures, 2MASS second incremental release NIR data, and X-ray imaging data to study trends in the NIR and X-ray properties of galaxy clusters. Our cluster sample is based on existing cluster samples (David et al. 1993; Mohr et al. 1999, hereafter MME; Reiprich & Böhringer 2002) and is limited by the incomplete sky coverage in the 2MASS second release ( $\sim 47\%$  of the sky). We return to the issue of sample selection and possible effects on our results in §2.2.2 & 5. The relevant cluster parameters (X-ray emission center, redshift  $z$ , X-ray emission weighted temperature  $T_X$ ) are gathered from the above references and others (Edge & Stewart 1991; White 2000). We only consider the clusters that have reliable  $T_X$  measurements and are reasonably beyond the galactic plane ( $|b| > 10^\circ$ ). The 2MASS second release contains 27 clusters for which luminosity functions can be estimated in the method described below. Among these 27 clusters, the ICM masses  $M_{ICM}$  of 13 were measured by MME, based on an analysis of ROSAT PSPC observations. We shall refer to these as the MME subsample. A list of our cluster sample appears in Table 1. In short, our cluster sample is at low redshift ( $0.016 \lesssim z \lesssim 0.09$  with mean redshift  $\sim 0.05$ ), and spans a range of X-ray emission weighted temperature ( $2.1 \leq T_X \leq 9.1$ ) that corresponds to about an order of magnitude in cluster binding mass ( $0.8 - 9 \times 10^{14} h_{70}^{-1} M_\odot$ ).

### 2.1. X-ray Estimate of Cluster Mass

We use an observed X-ray  $M - T_X$  relation to calculate the binding mass for each cluster. Finoguenov et al. (2001b) provide several  $M - T_X$  relations that arise from different subsets of a cluster ensemble. We use the relation obtained by fitting to the clusters with ASCA temperature profiles that are more massive than  $3.57 \times 10^{13} h_{70}^{-1} M_\odot$ ; all our clusters lie in this mass range. To be definite, we use

$$M_{500} = 2.55_{-0.25}^{+0.29} 10^{13} \frac{M_\odot}{h_{70}} \left( \frac{T_X}{1 \text{ keV}} \right)^{1.58_{-0.07}^{+0.06}} \quad (1)$$

where  $M_{500}$  is the mass enclosed by  $r_{500}$ , within which the mean overdensity is 500 times of the critical density of the universe  $\rho_c$ . Because our clusters are all low redshift, we neglect the effects of cosmic density evolution.

Within our fiducial cosmological model ( $\Omega_M = 0.3$  and  $\Omega_\Lambda = 0.7$ ) we calculate the cluster radius  $r_{500}$  and its angular extent  $\theta_{500} \equiv r_{500}/d_A$ , where  $d_A$  is the angular diameter distance. We analyze the galaxy and ICM properties within this region of the cluster. At the low redshift range spanned by our cluster sample the sensitivity to cosmology in the angular diameter distance is unimportant.

### 2.2. NIR Luminosity from 2MASS Data

Knowing the cluster angular extent, we search the 2MASS extended source catalog to identify cluster member galaxies. Among the three bands ( $J$ ,  $H$  and  $K_s$ ) 2MASS provides,  $K_s$  has been studied most extensively. For this reason we shall only consider the  $K_s$ -band (hereafter denoted as  $K$ -band for simplicity) in this paper. We use the “default”  $K_s$  magnitudes. The official 2MASS second release completeness limit for the default  $K_s$ -band is  $K_{lim} = 13.5$ <sup>5</sup>. However, after visual inspection of the magnitude distribution of the galaxies, we choose  $K_{lim} = 13.3$  as our completeness limit.

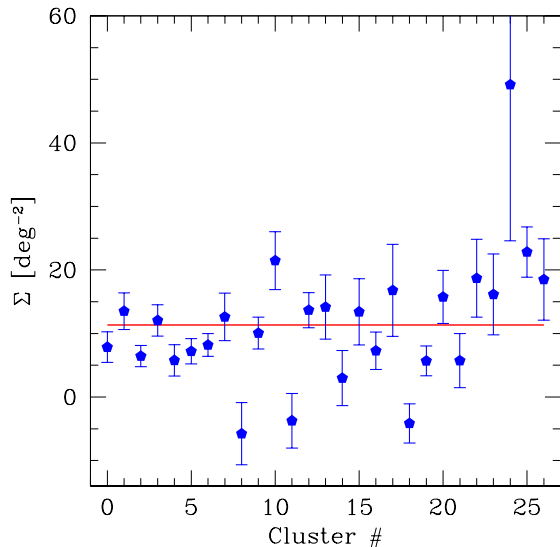


FIG. 1.— A comparison between the background galaxy surface density as obtained using the statistical method ( $\Sigma_{stat}$ , solid line), and the “annulus” method ( $\Sigma_{bgn}$ , solid points, see text)

### 2.2.1. Background Correction

To correct both the number counts and fluxes from background (and foreground; hereafter we refer to all non-cluster galaxies as background galaxies) galaxies in estimating the cluster NIR luminosity, we use the observed  $K$ -band galaxy brightness distribution  $d\Sigma_{stat}/dK$  (Kochanek et al. 2001). Integrating this quantity with respect to magnitude to our adopted 2MASS completeness limit gives the statistical galaxy surface density  $\Sigma_{stat}$ . This, multiplied by the cluster angular area  $\pi\theta_{500}^2$ , gives the expected number of background galaxies. The expected flux from the background galaxies is  $F_{stat} = \pi\theta_{500}^2 \int_{-\infty}^{K_{lim}} (d\Sigma_{stat}/dK) F dK$ , where  $F$  is the galaxy flux.

As a check of this statistical method, we also perform an “annulus” background correction; that is, for an assumed galaxy distribution profile with unknown normalization and a unknown constant background surface density, for each cluster we measure the number of galaxies within  $\theta_{500}$  ( $N_{cen}$ ) and within an annulus outside the cluster virial region ( $N_{ann}$ ), whose inner and outer radii are  $1.5\theta_{200}$  and  $3\theta_{200}$ , respectively, where  $\theta_{200} \equiv r_{200}/d_A$ . We convert between  $r_{200}$  and  $r_{500}$  using the “universal” dark matter distribution profile found in N-body simulations (Navarro et al. 1997, NFW); we use a fixed “concentration” parameter  $c = 5$ , and in that case  $r_{200} = 1.51 r_{500}$ .

Background and cluster galaxies lie in both the central and annular regions. Using the observables  $N_{cen}$  and  $N_{ann}$  and the NFW model for the distribution of galaxies, we estimate the normalizations of the cluster galaxy distribution and the uniform background galaxy surface density  $\Sigma_{bgn}$ . The number of cluster galaxies within  $\theta_{500}$  is then  $N_{cen} - \Sigma_{bgn} \pi\theta_{500}^2$ . For some clusters the annulus is only partially surveyed in the 2MASS second release, and we correct for this partial coverage. In some cases there are obvious galaxy clusterings (from visual inspection) in the annulus region; we avoid this possible contamination of the background annulus by other clusters or groups by excluding the area occupied by the clustering in the annulus.

Fig 1 contains a comparison of  $\Sigma_{stat}$  determined from the statistical approach and  $\Sigma_{bgn}$  as determined from the “annulus” method. There is general agreements between  $\Sigma_{stat}$  and  $\Sigma_{bgn}$ , indicating that local and statistical background corrections lead to the same results. For the analyses that follow, we adopt the statistical background surface density in making background corrections to the cluster galaxies. Note that, for 3 clusters,  $\Sigma_{bgn}$  determined from the “annulus” method is negative, which may either be due to the correction to the partially surveyed annulus region, or be due to a significant mismatch between the actual galaxy distribution in these clusters and the NFW model we are using. We have checked all the scaling relations presented in the following analysis using the local background estimate, and the changes to slope and normalization all lie within the  $1\sigma$  uncertainties.

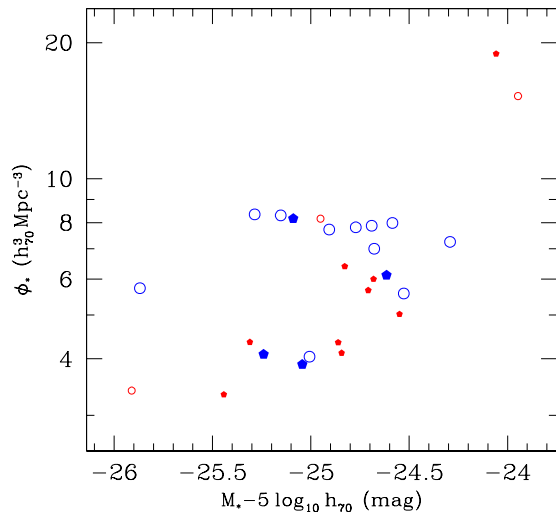


FIG. 2.— Measured  $M_*$  and  $\phi_*$  for our cluster sample (see Table 1). Solid circles are clusters with  $kT \geq 4$  keV. Larger symbols denote clusters with  $z \leq 0.05$ , while smaller symbols refer to  $z > 0.05$  clusters.

### 2.2.2. Luminosity Function

We transform the apparent magnitudes into solar luminosities using  $K_{\odot} = 3.39$  (Kochanek et al. 2001), the cluster distance and Galactic extinction:

$$M_K = K - 25 - 5 \log_{10}(d_L/1\text{Mpc}) - A_K, \quad (2)$$

<sup>5</sup><http://www.ipac.caltech.edu/2mass/releases/second/doc/explsup.html>

TABLE 1  
BASIC DESCRIPTIONS OF THE CLUSTERS

(1)	(2)	(3)	(4)	(5)	(6)	(7)	(8)	(9)	(10)
Name	$z$	$T_X$ (keV)	$N_{gal}$	$\phi_*$ ( $h_{70}^3 \text{ Mpc}^{-3}$ )	$M_* - 5 \log h_{70}$ (mag)	$L_{500}$ ( $h_{70}^{-2} 10^{11} L_\odot$ )	$\Upsilon_{500}$ ( $h_{70} \Upsilon_\odot$ )	$f_{star}$ ( $10^{-2}$ )	$f_{ICM}$ ( $10^{-2}$ )
A85	0.0556	$6.1_{-0.12}^{+0.12}$	27	$5.26_{-1.81}^{+1.81}$	$-24.71 \pm 0.18$	$7.97 \pm 0.03$	$55_{-14}^{+14}$	$1.41_{-0.46}^{+0.46}$	$14.92 \pm 0.39$
A119	0.0440	$5.8_{-0.36}^{+0.36}$	39	$3.80_{-1.28}^{+1.28}$	$-25.24 \pm 0.20$	$8.32 \pm 0.05$	$49_{-13}^{+13}$	$1.58_{-0.53}^{+0.53}$	$12.03 \pm 0.75$
A262	0.0161	$2.41_{-0.03}^{+0.03}$	41	$7.31_{-2.37}^{+2.37}$	$-24.69 \pm 0.27$	$2.51 \pm 0.04$	$40_{-10}^{+10}$	$1.76_{-0.57}^{+0.57}$	$10.17 \pm 0.39$
A496	0.0328	$3.91_{-0.04}^{+0.04}$	40	$7.41_{-2.37}^{+2.37}$	$-24.59 \pm 0.20$	$4.96 \pm 0.03$	$44_{-11}^{+11}$	$1.71_{-0.55}^{+0.55}$	$13.47 \pm 0.32$
A644	0.0704	$6.59_{-0.1}^{+0.1}$	17	$5.57_{-1.30}^{+1.30}$	$-24.68 \pm 0.19$	$8.45 \pm 0.03$	$59_{-15}^{+15}$	$1.33_{-0.34}^{+0.34}$	$13.04 \pm 0.47$
A754	0.0528	$8.5_{-0.3}^{+0.3}$	44	$4.04_{-1.30}^{+1.30}$	$-24.86 \pm 0.16$	$10.99 \pm 0.03$	$68_{-17}^{+17}$	$1.17_{-0.38}^{+0.38}$	$13.90 \pm 1.50$
A1367	0.0216	$3.5_{-0.11}^{+0.11}$	59	$7.25_{-2.24}^{+2.24}$	$-24.77 \pm 0.20$	$4.42 \pm 0.03$	$41_{-10}^{+10}$	$1.79_{-0.58}^{+0.58}$	$11.85 \pm 0.45$
A1651	0.0850	$6.3_{-0.31}^{+0.31}$	8	$17.55_{-8.81}^{+8.81}$	$-24.06 \pm 0.17$	$13.89 \pm 0.01$	$35_{-10}^{+10}$	$2.33_{-0.88}^{+0.88}$	$13.69 \pm 0.70$
A2255	0.0800	$6.8_{-0.2}^{+0.2}$	16	$3.36_{-1.30}^{+1.30}$	$-25.30 \pm 0.21$	$9.81 \pm 0.06$	$54_{-14}^{+14}$	$1.45_{-0.53}^{+0.53}$	$13.14 \pm 2.60$
A2319	0.0564	$9.1_{-0.09}^{+0.09}$	61	$5.95_{-1.80}^{+1.80}$	$-24.83 \pm 0.12$	$17.30 \pm 0.02$	$48_{-12}^{+12}$	$1.65_{-0.38}^{+0.38}$	$16.69 \pm 0.52$
A3266	0.0594	$6.2_{-0.4}^{+0.4}$	30	$4.92_{-1.73}^{+1.73}$	$-25.03 \pm 0.18$	$9.94 \pm 0.04$	$45_{-13}^{+13}$	$1.71_{-0.53}^{+0.53}$	$16.66 \pm 1.31$
A3558	0.0480	$5.7_{-0.12}^{+0.12}$	61	$7.59_{-2.30}^{+2.30}$	$-25.09 \pm 0.14$	$13.91 \pm 0.03$	$28_{-7}^{+7}$	$2.72_{-0.88}^{+0.88}$	$15.83 \pm 0.38$
A4038	0.0283	$3.15_{-0.03}^{+0.03}$	32	$6.50_{-2.15}^{+2.15}$	$-24.68 \pm 0.24$	$3.23 \pm 0.04$	$48_{-12}^{+12}$	$1.53_{-0.38}^{+0.38}$	$11.64 \pm 0.73$
A133	0.0569	$3.8_{-0.56}^{+0.56}$	13	$14.15_{-6.94}^{+6.94}$	$-23.95 \pm 0.22$	$4.97 \pm 0.02$	$42_{-15}^{+15}$	$1.79_{-0.75}^{+0.75}$	–
A548e	0.0410	$3.1_{-0.1}^{+0.1}$	31	$7.71_{-3.57}^{+3.57}$	$-25.15 \pm 0.22$	$5.72 \pm 0.05$	$26_{-7}^{+7}$	$2.78_{-0.90}^{+0.90}$	–
A1185	0.0304	$3.9_{-0.1}^{+0.1}$	27	$4.01_{-2.41}^{+2.41}$	$-24.81 \pm 0.37$	$3.25 \pm 0.06$	$67_{-34}^{+34}$	$1.12_{-0.62}^{+0.62}$	–
A1650	0.0845	$6.7_{-0.5}^{+0.5}$	6	$4.66_{-2.60}^{+2.60}$	$-24.55 \pm 0.26$	$6.74 \pm 0.04$	$76_{-35}^{+35}$	$1.03_{-0.40}^{+0.40}$	–
A1767	0.0701	$4.1_{-0.8}^{+0.8}$	7	$3.83_{-2.51}^{+2.51}$	$-24.84 \pm 0.39$	$3.96 \pm 0.07$	$59_{-27}^{+27}$	$1.27_{-0.64}^{+0.64}$	–
A2107	0.0421	$4.31_{-0.35}^{+0.35}$	22	$3.61_{-1.53}^{+1.53}$	$-25.04 \pm 0.28$	$4.53 \pm 0.06$	$56_{-16}^{+16}$	$1.35_{-0.47}^{+0.47}$	–
A2147	0.0351	$4.91_{-0.18}^{+0.18}$	42	$5.69_{-1.84}^{+1.84}$	$-24.62 \pm 0.19$	$5.19 \pm 0.03$	$60_{-15}^{+15}$	$1.27_{-0.42}^{+0.42}$	–
A2151	0.0370	$2.4_{-0.06}^{+0.06}$	23	$5.32_{-1.84}^{+1.84}$	$-25.87 \pm 0.29$	$5.18 \pm 0.14$	$19_{-4}^{+4}$	$3.65_{-1.18}^{+1.18}$	–
A2440	0.0904	$3.88_{-0.16}^{+0.16}$	7	$3.11_{-1.55}^{+1.55}$	$-25.79 \pm 0.34$	$6.15 \pm 0.15$	$35_{-9}^{+9}$	$2.14_{-0.72}^{+0.72}$	–
A2589	0.0416	$3.7_{-0.69}^{+0.69}$	19	$6.74_{-3.38}^{+3.38}$	$-24.29 \pm 0.29$	$3.39 \pm 0.03$	$59_{-23}^{+23}$	$1.27_{-0.56}^{+0.56}$	–
A2593	0.0433	$3.1_{-0.9}^{+0.9}$	23	$7.17_{-4.37}^{+4.37}$	$-24.91 \pm 0.28$	$4.56 \pm 0.05$	$33_{-17}^{+17}$	$2.22_{-0.84}^{+0.84}$	–
A2626	0.0573	$2.9_{-0.5}^{+0.5}$	14	$7.58_{-5.46}^{+5.46}$	$-24.95 \pm 0.34$	$4.70 \pm 0.07$	$29_{-10}^{+10}$	$2.52_{-0.54}^{+0.54}$	–
A2634	0.0312	$3.7_{-0.18}^{+0.18}$	27	$5.18_{-1.83}^{+1.83}$	$-24.53 \pm 0.26$	$3.33 \pm 0.03$	$60_{-16}^{+16}$	$1.24_{-0.62}^{+0.62}$	–
A3389	0.0265	$2.1_{-0.6}^{+0.6}$	27	$8.27_{-4.92}^{+4.92}$	$-25.05 \pm 0.31$	$3.29 \pm 0.07$	$24_{-12}^{+12}$	$2.82_{-1.56}^{+1.56}$	–

Note. — Columns: (1) Name; (2) Redshift; (3) Emission-weighted mean temperature; (4) Estimated number of member galaxies; (5) Characteristic number density; (6) Characteristic magnitude; (7) Total luminosity within  $r_{500}$ ; (8)  $K$ -band mass-to-light ratio; (9) Stellar mass fraction; (10) ICM mass fraction. Uncertainties in all columns quoted at  $1\sigma$  level.  $M_*$  &  $\phi_*$  calculated assuming  $\alpha = -1.1$ . All calculations done with  $h_{70} = 1$ .

where  $d_L$  is the luminosity distance, and  $A_K$  accounts for the Galactic extinction. We ignore  $k$ -corrections, because our clusters are all at very low redshifts. The Galactic extinction, which has a small effect on the overall luminosity, is assumed to be the same for the entire cluster; we obtain the extinction values from the NASA/IPAC Extragalactic Database .

Using the NFW model with concentration  $c = 5$ , we deproject to convert the projected number and luminosity  $L_{obs}$  of galaxies within  $r_{500}$ . The deprojection essentially reduces the background corrected luminosity and number by 20 – 30%. These quantities divided by the cluster volume  $V_{cls} = (4\pi/3)r_{500}^3$  are the cluster mean number density  $n_{obs}$  and luminosity density  $j_{obs}$ , which are related to the cluster luminosity function  $\phi(L)$ :

$$n_{obs} = \int_{L_{lim}}^{\infty} \phi(L) dL \quad \text{and} \quad j_{obs} = \int_{L_{lim}}^{\infty} L \phi(L) dL, \quad (3)$$

where  $L_{lim}$  is the luminosity corresponding to  $K_{lim}$  for each particular cluster. We use the Schechter (1976) form for the luminosity function:

$$\phi(L) dL = \phi_* \left( \frac{L}{L_*} \right)^\alpha e^{-L/L_*} d \left( \frac{L}{L_*} \right), \quad (4)$$

where  $L_*$  and  $\phi_*$  are characteristic luminosity and number densities, respectively, and  $\alpha$  is the faint-end power law index.

In practice, the 2MASS data do not go deep enough to provide useful constraints on the faint end slope  $\alpha$  for all of our clusters. Thus, we use external constraints to set

$\alpha$ . The NIR cluster Schechter function faint end slope is generally found to be  $-1.3 \lesssim \alpha \lesssim -0.8$  (e.g. Mobasher & Trentham 1998; Andreon & Pelló 2000; Tustin et al. 2001; Balogh et al. 2001a; De Propris et al. 2002). In the following we adopt  $\alpha = -1.1$ . (We discuss the effect of different  $\alpha$  on our results in §5.) Given  $n_{obs}$ ,  $j_{obs}$ ,  $\alpha$  and  $L_{lim}$ , we solve for  $\phi_*$  and  $L_*$  using Eqn 3.

Fig 2 contains the derived  $\phi_*$  and  $M_*$  (the absolute magnitude corresponding to  $L_*$ ). The distribution of  $M_*$  ( $\overline{M_*} - 5 \log h_{70} = -24.88 \pm 0.02$ ) in Fig 2 and Table 1 shows no clear correlation with cluster mass or redshifts, but many nearby clusters exhibit larger  $\phi_*$ . Our cluster sample is based on existing X-ray cluster catalogs, and so there is a tendency for the low temperature systems to lie at low redshift. For example, the mean redshift of the lower temperature half of the sample (i.e.  $kT_X < 4$  keV) is  $0.040 \pm 0.001$  as compared to  $0.060 \pm 0.001$  for the other half. This could potentially pose a problem, because any redshift related systematic could masquerade as a mass related trend in our cluster population. We probe for systematics by examining the luminosity function parameters within the hot and cold cluster subsamples. Dividing each subsample at redshift 0.05, we find no statistically significant differences with redshift in  $\overline{M_*}$  or  $\overline{\phi_*}$  for either of the subsamples. However, within the same redshift range,  $\overline{\phi_*}$  is significantly higher for the low temperature subsample, consistent with the shallow light-mass relation presented above.

In obtaining the Schechter parameters by using the observed light and number of galaxies, we do not consider the brightest cluster galaxy (BCG), which typically contains a

significant fraction of the cluster light and would bias the parameters of the cluster luminosity function. We account for the BCG light separately, modeling cluster luminosity functions with Schechter functions plus the light of the BCG. There are two clusters whose Schechter parameters appear to be different from that of other clusters: A133 & A1651. Their  $M_*$  are relatively dim, and their  $\phi_*$  about twice as large as others. This may be because of their relatively small number of member galaxies, and their extraordinarily bright central dominant galaxies: removal of the luminosity contribution from the BCGs dramatically reduces  $L_*$  and boosts  $\phi_*$ . These two clusters underscore the fact that our integral approach to solving for  $L_*$  and  $\phi_*$  leads to correlated errors in  $L_*$  and  $\phi_*$  that maintain an accurate estimate of the total cluster light even when estimates of  $L_*$  and  $\phi_*$  individually can be quite inaccurate.

### 2.2.3. Estimating Total Light and Stellar Mass

With the Schechter parameters  $\phi_*$  and  $L_*$ , we estimate the total cluster luminosity by integrating over the luminosity function:  $L_{tot} = V_{cls} L_* \phi_* \Gamma(\alpha + 2) + L_{bcg}$ . To reduce the dependence of our light estimate on the faint end slope parameter  $\alpha$  we truncate the luminosity function at the absolute magnitude  $M_{low} = -20$ :

$$j'_{tot} = L_{bcg}/V_{cls} + \int_{L_{low}}^{\infty} L \phi(L) dL. \quad (5)$$

For our sample and choice of  $\alpha$ ,  $j'_{tot}$  differs from  $j_{tot}$  only at 2 – 3% level. In the analyses that follow we make no distinction between these two, and use the “truncated” luminosity as our luminosity estimate throughout.

We also apply a correction for the fact that the the default 2MASS magnitudes underestimate the total light of the galaxies. By comparing the 2MASS default (isophotal) magnitudes of their galaxy sample with the total magnitudes of deep photometry (Pahre 1999), Kochanek et al. (2001) found a systematic difference of 20%. We multiply  $L_{tot}$  by the same factor of 1.2.

To obtain the total stellar mass, we multiply the total luminosity  $L_{tot}$  by the average stellar mass-to-light ratio  $\bar{\Upsilon}_{star}(T_X)$  for each cluster. We estimate the mean stellar mass-to-light ratio from the observations of elliptical and spiral galaxies (Gerhard et al. 2001; Bell & de Jong 2001), and take into account the varying spiral fraction as a function of cluster temperature (Bahcall 1977b; Dressler 1980, notice that the spiral fractions were determined using  $B$ -band light rather than  $K$ -band; we neglect possible wavelength dependence of the spiral fraction here). The details of our approach are presented in the Appendix. We show in Fig 3 the resulting mean stellar mass-to-light ratio  $\bar{\Upsilon}_{star}$ , and compare it with the result from the 2dF galaxy redshift survey (Cole et al. 2001), which was obtained by using the observed galaxy colors and redshifts to constrain their evolution, based on the recent version of a population synthesis code (Bruzual A. & Charlot 1993). This value  $0.73\Upsilon_{\odot}$  (where  $\Upsilon_{\odot}$  is the solar  $K$ -band mass-to-light ratio) is consistent with our lowest temperature clusters (highest spiral fraction), but over the full range of cluster masses examined in this sample, the stellar mass-to-light ratio is expected to vary by  $\sim 10\%$ .

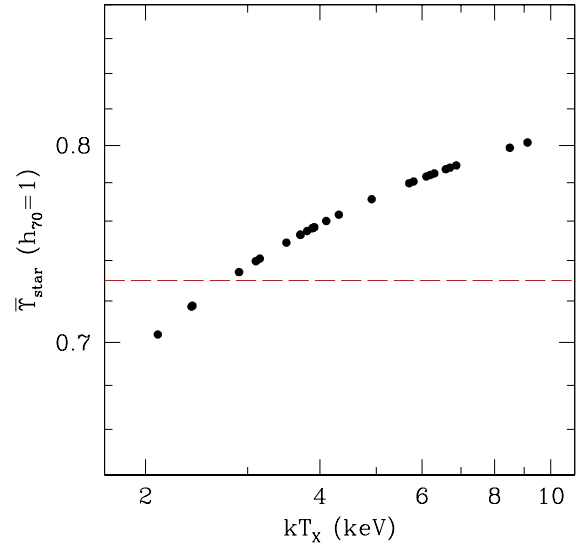


FIG. 3.— The  $K$ -band mean stellar mass-to-light ratio  $\bar{\Upsilon}_{star}(T_X)$  based on the observed mass-to-light ratio in elliptical and spiral galaxies and spiral fractions in clusters. See Appendix for more details. The dashed-line is the mean value from the 2dF survey (Cole et al. 2001)  $\bar{\Upsilon}_{star,2dF} = 0.73\Upsilon_{\odot}$ , assuming a Kennicutt (1983) initial mass function.

### 2.3. Estimating the ICM Mass from X-ray Emission

We calculate the ICM mass for the 13 clusters in the MME subsample using fits to the ROSAT Position Sensitive Proportional Counter (PSPC) X-ray surface brightness fits from the literature (Mohr et al. 1999). The 0.5:2.0 keV X-ray emissivity is relatively insensitive to temperatures (varying by 10% for a factor of two increase in temperature for clusters with temperatures above 1.5 keV), so one needs not know the cluster temperature profile to determine the ICM density profile from an X-ray image. We have adjusted the density profiles to reflect improved temperature measurements in two of the clusters. Analysis of mock PSPC images of simulated galaxy clusters indicates that cluster ICM masses can be estimated with an accuracy of  $\sim 10\%$  (Mohr et al. 1999) and that clumping in the ICM enhances the X-ray emissivity leading to an estimated  $\sim 10\%$  bias in ICM mass estimates (Mohr et al. 1999; Mathiesen et al. 1999). We correct for this bias by reducing ICM mass estimates for all 13 clusters by 10%. However, this reduction is counterbalanced when one considers the  $\sim 10\%$  diminution of the cluster baryon fraction at  $r_{500}$  compared to the global baryon fraction  $\Omega_b/\Omega_M$  as seen in numerical studies, where  $\Omega_b$  is the total baryon density in the universe. We recalculate the ICM masses for this analysis using the  $M_{500} - T_X$  relation adopted for the rest of the analysis (Finoguenov et al. 2001b, see Eqn 1).

## 3. NIR LUMINOSITY AND COSMOLOGY

One critical issue for ongoing NIR cluster surveys is determining the degree to which the NIR light from the stellar populations within cluster galaxies traces the galaxy cluster binding mass. Cluster binding mass or virial mass is central to using the abundance of galaxy clusters to constrain cosmology (although deep surveys contain enough

information to solve for cluster binding mass and cosmology simultaneously; Majumdar & Mohr 2002). If NIR galaxy light is a good indicator of cluster binding mass, then large solid angle surveys like 2MASS could be used to (1) define very large samples of clusters in the nearby universe (see Kochanek et al. 2002), and (2) provide direct constraints on a combination of the local power spectrum of density fluctuations and the mean matter density. Due to the limited size of our sample, we simply focus on the relation between the virial mass (inferred from X-ray observations) and stellar luminosity (obtained from 2MASS photometry) of nearby clusters, discussing the implications for future NIR cluster surveys. In addition, we use the NIR light and measurements of cluster ICM masses to address the baryon fraction, the cluster mass-to-light ratio, and the cosmological matter density parameter.

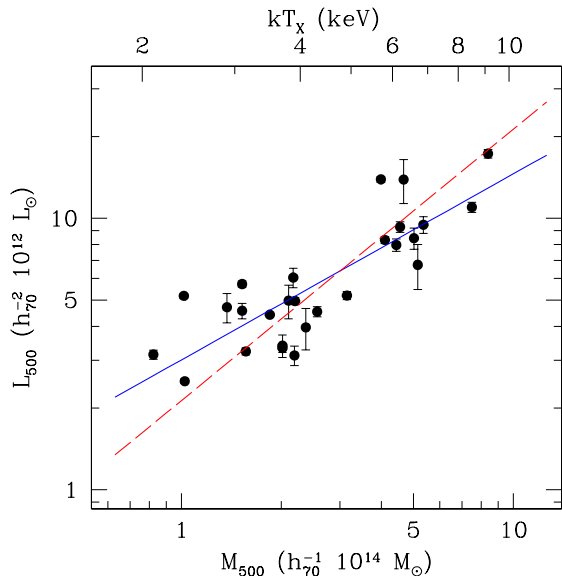


FIG. 4.— The cluster  $K$ -band luminosity–mass correlation. The uncertainties in  $L_{500}$  are rather small, typically less than 10% (see Table 1). The solid line shows the best-fit relation of slope of 0.69 (Eqn 6), while the dashed line shows a slope of 1.0 behavior.

Figure 4 contains a plot of NIR light  $L_{500}$  versus the binding mass  $M_{500}$ , corresponding to the light and mass contained within the cluster radius  $r_{500}$ . We use Eqn 1 to estimate  $M_{500}$ , with the cluster emission-weighted mean temperature  $T_X$  taken from the literature. The corresponding temperature scale is presented at the top of the figure. For our sample of 27 nearby clusters there is a reasonably tight correlation between cluster mass and  $K$ -band light

$$L_{500} = 6.4 \pm 0.4 \times 10^{12} \frac{L_{\odot}}{h_{70}^2} \left( \frac{M_{500}}{3 \times 10^{14} h_{70}^{-1} M_{\odot}} \right)^{0.69 \pm 0.09}. \quad (6)$$

The best-fit results in this paper are obtained by minimizing the vertical distances in log space to the line from the data points, and no uncertainties in  $M_{500}$  are included in the fitting procedure. The  $1\sigma$  uncertainties are determined by bootstrap resampling and refitting  $10^3$  times. As implied by the equation, the pivot point for the fit is at  $3 \times 10^{14} h_{70}^{-1} M_{\odot}$ , roughly corresponding to 4.8 keV.

The best-fit correlation (solid line) differs from  $L_{500} \propto M_{500}$  (dashed line) by  $\sim 3\sigma$ , indicating a

mass-to-light ratio that increases with mass. In essence, low mass clusters produce relatively more light per unit binding mass than high mass clusters. Possible explanations include a higher star formation efficiency in low mass clusters (see §4.1) or a stripping process that liberates stars from galaxies more efficiently in high mass than in low mass clusters (e.g. Trentham & Mobasher 1998; Gregg & West 1998). As discussed in §1, we do not expect the  $K$ -band stellar mass-to-light ratio to be very sensitive to stellar population and star formation history variations, but gross differences in the stellar populations of low and high mass clusters could in principle contribute to the shallow NIR light–mass relation found here. We return to this issue in §4.

The fractional scatter in  $L_{500}$  about this best fit relation is 28%, suggesting that  $K$ -band light does indeed provide a useful tracer of cluster mass. Possible sources of the scatter include: the variations in the cluster star formation and galaxy formation history, variations in the faint-end slope of the luminosity function  $\alpha$ , the scatter ( $\sim 17\%$ ) in the adopted  $M - T_X$  relation, the projection of unusually bright background galaxies onto the clusters, and the “deprojection” of the cluster luminosity (i.e. deviations from spherical symmetry and from the assumed galaxy distribution model). In practice, the uncertainty in binding mass estimates will depend on the filter used to detect and characterize clusters. Crudely speaking, using the slope and amplitude of the scaling relation, for a given  $K$ -band light, one could predict the galaxy cluster mass with a statistical accuracy of  $\sim 45\%$ . Of course this is likely a lower limit to the true mass uncertainties in a NIR cluster survey, because in practice one will not know the apparent virial radius  $\theta_{500}$  and cluster position *a priori*.

Figure 5 contains the  $K$ -band mass-to-light ratio versus binding mass  $M_{500}$ . The trend of increasing  $K$ -band mass-to-light ratio  $\Upsilon_{500}$  is best fitted by

$$\Upsilon_{500} = 47 \pm 3 h_{70} \Upsilon_{\odot} \left( \frac{M_{500}}{3 \times 10^{14} h_{70}^{-1} M_{\odot}} \right)^{0.31 \pm 0.09}. \quad (7)$$

The Spearman correlation coefficient for the fit is 0.63, with a  $1.6 \times 10^{-3}$  probability of being consistent with no correlation. The average mass-to-light ratio over all clusters is  $47 \pm 3 h_{70} \Upsilon_{\odot}$  (short dashed line) and the average for clusters with  $kT_X \geq 3.7$  keV (more massive than  $2 \times 10^{14} h_{70}^{-1} M_{\odot}$ ) is  $53 \pm 3 h_{70} \Upsilon_{\odot}$ . A fit to the clusters with  $kT_X \geq 3.7$  keV produces a slope that is consistent with zero ( $0.03 \pm 0.12$ ), which is one way of demonstrating that much of the leverage on the slope comes from the low mass systems. The 8 clusters that have  $kT_X < 3.7$  keV are of low redshift ( $0.016 \leq z \leq 0.057$ ,  $\bar{z} = 0.034$ ). Because visual inspections of these cluster fields do not show unusual behavior relative to higher  $T_X$  clusters (e.g. deficiency of galaxies), we believe the low  $\Upsilon_{500}$  for these low  $T_X$  clusters is robust.

In general, trends in blue/visual band mass-to-light ratio with temperature have not been seen (e.g. Hradecky et al. 2000; David et al. 1995), but more recently both Bahcall & Comerford (2002) and Girardi et al. (2002) reported positive correlations between cluster blue band ( $V$  and  $B$ , respectively) mass-to-light ratio and temperature. Bahcall & Comerford (2002) observed  $\Upsilon_V \propto T_X^{0.3 \pm 0.1}$ , which is somewhat shallower than the trend we see in our sample

( $\Upsilon_K \propto T_X^{0.5 \pm 0.1}$ ); the best-fit of Girardi et al. (2002) sample is  $\Upsilon_B \propto M^{0.25}$ . Our results are statistically consistent with these other relations. Bahcall & Comerford (2002) interpret the dependence on temperature as an aging effect in the stellar population. If that is the case, then one would expect this trend to be less prominent in the NIR, where for old stellar populations the stellar mass-to-light ratio is relatively insensitive to population age. Because we see the trend in the  $K$ -band, it is certainly possible that there is an underlying variation in star formation efficiency over cluster mass scales (we examine this possibility in §4.1).

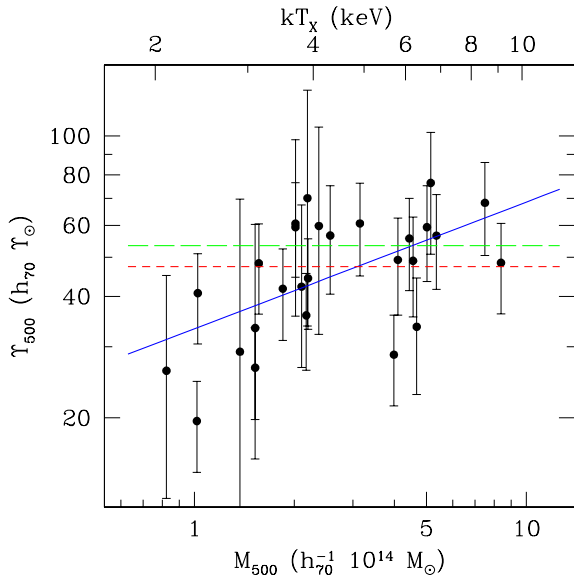


FIG. 5.— The cluster  $K$ -band mass-to-light ratio vs cluster mass. The solid line is the best-fit relation Eqn 7, the short-dashed line is the average of all clusters –  $47 \pm 3 h_{70} \Upsilon_{\odot}$ , and the long-dashed line is the average of hot ( $kT_X \geq 3.7$  keV, or  $M_{500} \gtrsim 2 \times 10^{14} h_{70}^{-1} M_{\odot}$ ) clusters –  $53 \pm 3 h_{70} \Upsilon_{\odot}$ . The error bars mainly reflect the uncertainties in cluster binding mass estimated from  $T_X$ .

Our results are consistent with the  $K$ -band mass-to-light ratio found in a detailed spectroscopic and 2MASS photometric study of the Coma cluster ( $T_X = 8.21 \pm 0.16$  keV):  $\Upsilon = (68 \pm 21) h_{70} \Upsilon_{\odot}$  (Rines et al. 2001, when converted from their projected mass-to-light ratio to the “deprojected” mass-to-light ratio adopted in our analysis). Interestingly, Kochanek et al. (2002) find a weakly decreasing mass-to-light ratio using 2MASS data. Evaluating cluster  $K$ -band light at  $r_{200}$ , they find  $\Upsilon_{200} \propto M_{200}^{-0.10 \pm 0.09}$ , which is inconsistent with our results at about the  $4\sigma$  level. Their approach relies on a pseud-matched filter cluster finding algorithm using an NFW model with fixed virial radius and constant  $L_*$  and  $\alpha$ . The number of galaxies within the cluster virial region  $N_{*666}$  is estimated by rescaling the number observed using a fixed virial radius NFW filter. They show that  $N_{*666}$  is correlated with several estimators of binding mass. Although both our approach and theirs should, in principle, give consistent results, we believe our method offers several advantages for studies of the  $K$ -band light – virial mass relationship. First, we start with a proven, low scatter X-ray estimator of cluster virial mass, and we use X-ray emission peaks as the cluster center. Thus, we know the size and location of our cluster virial region, whereas in their approach they have to pull these quantities from the

2MASS data and bootstrap to an estimate of the total cluster light. Second, we use the NFW model only in deprojecting the cluster light, whereas their cluster detection algorithm is built upon the NFW model. Thus, our method would be less affected by deviations in some clusters from the NFW model.

### 3.1. Cluster Mass-to-Light Ratio Constraint on $\Omega_M$

Cluster scale mass-to-light ratios  $\Upsilon_{500}$ , together with observations of the mean luminosity density of the universe  $\bar{j}$ , have often been used to estimate the mean matter density  $\bar{\rho}$  or matter density parameter  $\Omega_M$  (e.g. Bahcall 1977a; Trimble 1987; Bahcall et al. 1995; Carlberg et al. 1996; Rines et al. 2001; Bahcall & Comerford 2002; Girardi et al. 2002, among others). Taking the mean mass-to-light ratio of the universe to be  $\Upsilon_{univ} = \bar{\rho}/\bar{j}$ , then  $\Omega_M \approx \bar{j} \Upsilon_{500} / \rho_c$ , if the cluster mass-to-light ratio is equal to the universal mass-to-light ratio. A potential weakness of this approach is that the galaxy populations inside and outside galaxy clusters differ significantly, with field galaxies being predominantly late type with a mix of young and old stellar populations and cluster galaxies being predominantly early type with mostly old stellar populations (e.g. Dressler 1984). With these dramatic galaxy population differences, it is not clear that the star formation efficiency within clusters would be representative of that in the universe as a whole. Nevertheless, an application of this technique using  $K$ -band light is particularly interesting, because it minimizes mass-to-light ratio differences due to the ages of stellar populations. Perhaps most interesting is that in combination with external constraints on the matter density parameter, these results will provide insights into the star formation history in clusters as compared to the universe as a whole (see §3.3).

Because the  $K$ -band cluster mass-to-light ratio is an increasing function of cluster mass, we will evaluate  $\Omega_M$  by using both the mean  $\bar{\Upsilon}_{500,all} = (47 \pm 3) h_{70} \Upsilon_{\odot}$  of all clusters, and the mean mass-to-light ratio of  $T_X \geq 3.7$  keV clusters,  $\bar{\Upsilon}_{500,hot} = (53 \pm 3) h_{70} \Upsilon_{\odot}$ . For the mean luminosity density, we adopt the value obtained by Kochanek et al. (2001):  $\bar{j} = (5.00 \pm 0.52) \times 10^8 h_{70} L_{\odot} \text{Mpc}^{-3}$ . Combining  $\bar{\Upsilon}_{500,all}$  or  $\bar{\Upsilon}_{500,hot}$  with  $\bar{j}$ , with the critical density  $\rho_c = 1.36 \times 10^{11} h_{70}^2 M_{\odot} \text{Mpc}^{-3}$ , we estimate the matter density parameter  $\Omega_M = 0.17 \pm 0.02$  (whole sample) or  $\Omega_M = 0.19 \pm 0.03$  (hot cluster subsample).

### 3.2. Total Baryon Fraction Constraint on $\Omega_M$

Another way of constraining the mean matter density of the universe from the clusters is by using the baryon fraction in galaxy clusters to estimate the universal baryon fraction. In combination with external constraints on the baryon density parameter, one can then estimate the matter density parameter (e.g. White et al. 1993b; David et al. 1995; Evrard 1997, MME). Hydrodynamical simulations indicate that the ICM is more extended in its distribution than the cluster dark matter, and so corrections for this “depletion” effect must be included. In addition, hydro simulations indicate that clumping and substructure in the ICM enhance the X-ray emission relative to that expected if the gas were smoothly distributed (MME; Mathiesen et al. 1999). A correction for this “clumping” effect must also be included.

Here we only consider the two dominant baryon reservoirs in galaxy clusters: stars in the galaxies and the hot ICM (that is, we do not specifically include a contribution of the interstellar medium in galaxies, intergalactic stars or dark baryonic objects). We write the cluster baryon fraction as  $f_b \equiv (M_{star} + M_{ICM})/M_{500}$ , where  $M_{star}$  and  $M_{ICM}$  are the total stellar and ICM mass inside  $r_{500}$ , respectively, and we have corrected the ICM contribution for depletion and clumping (see §2.3). We estimate  $M_{star}$  using the  $K$ -band luminosity (see §2.2.3). If the corrected cluster baryon fraction then reflects the global one, we have  $\Omega_M = \Omega_b/f_b$ .

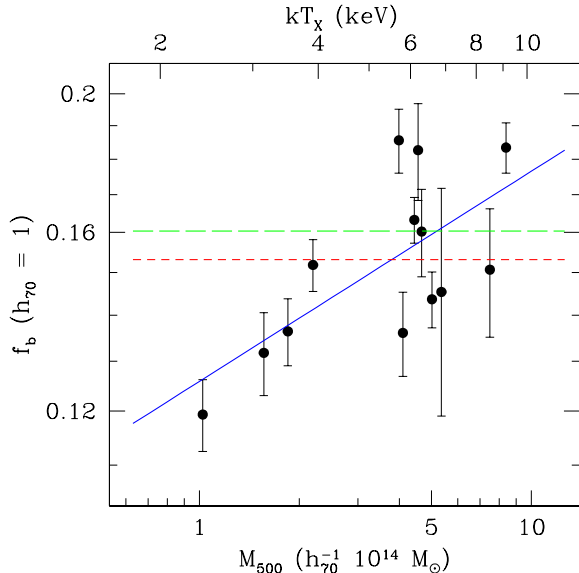


FIG. 6.— The baryon fraction  $f_b$  as a function of cluster mass for the 13 2MASS clusters in the MME subsample. The long-dashed line is the mean of the 10 clusters that have  $kT_X \geq 3.7$  keV,  $\bar{f}_{b,hot} = 0.160$ . The short-dashed line is the mean for all 13 clusters,  $\bar{f}_{b,all} = 0.153$ .

We show in Fig 6 the total baryon fraction in our cluster sample, which is an increasing function of cluster mass. The best-fit is

$$f_b = 0.148^{+0.005}_{-0.004} \left( \frac{M_{500}}{3 \times 10^{14} M_{\odot}} \right)^{0.148 \pm 0.04} \quad (8)$$

for  $h_{70} = 1$ . Note that this sample includes only 13 clusters – namely, those clusters in our ensemble that also lie in the MME X-ray flux limited sample of 45 clusters. The increase in the baryon fraction with cluster mass mainly reflects the dependence of the ICM mass fraction on cluster mass, because the ICM mass dominates over the stellar mass in galaxy clusters (we examine this issue in §4.2 below). This correlation between ICM mass and temperature was noted by MME, whose study favors the trend  $M_{ICM}/M_{500} \propto T_X^{0.34 \pm 0.22}$ , which is a likely indication of preheating (e.g. Bialek et al. 2001) or perhaps variations in star formation efficiency (Bryan 2000). Because our depletion correction from hydrodynamical simulations is most appropriate for massive clusters, and because massive clusters are the systems that sample the largest portions of the universe, we take the baryon fraction in our massive systems as most representative of the universal baryon fraction. In fact, the best-fit slope for the  $f_b - T_X$  relation of the hot ( $kT_X \geq 3.7$  keV) clusters in this subsample is

much shallower and consistent with zero:  $0.054 \pm 0.152$ , which may be an indication of the cluster baryon fraction asymptotically approaches the universal baryon fraction. Following the approach of the last section, we will present constraints on the density parameter that arise from the average characteristics of the entire subsample and the hot clusters in this subsample (10 clusters).

The mean baryon fraction for the 10 clusters with  $kT_X \geq 3.7$  keV is  $\bar{f}_{b,hot} = 0.160 \pm 0.006$ , and for the whole MME subsample we have  $\bar{f}_{b,all} = 0.153 \pm 0.006$ . We do not present the  $h$  scaling, because  $M_{star}$  and  $M_{ICM}$  scale with the Hubble constant differently. With the value of  $\Omega_b h_{70}^2 = 0.0457 \pm 0.0018$  from *WMAP* measurements, we estimate  $\Omega_M$ ; for the hot clusters in the subsample we get  $\Omega_M = 0.28 \pm 0.03$ , while for the whole MME subsample  $\Omega_M = 0.30 \pm 0.03$ . This value is consistent with the previous results using the same technique. Evrard (1997) deduced that  $\Omega_M < 0.40$  using the previous X-ray observations. Based on ICM mass fraction measurements of 45 & 30 clusters, MME and Ettori & Fabian (1999) concluded that  $\Omega_M < 0.32$  &  $0.34$ , respectively. Grego et al. (2001) estimated  $\Omega_M \sim 0.25$  from the SZE observations of 18 clusters. Finally, with Chandra observations of 7 intermediate redshift clusters, Allen et al. (2002) deduced that  $\Omega_M = 0.30^{+0.04}_{-0.03}$ .

### 3.3. Comparison of $\Omega_M$ Constraints

Our baryon fraction estimate of  $\Omega_M$  is in excellent agreement with *WMAP* constraints from the CMB anisotropy:  $\Omega_M(f_b) = 0.28 \pm 0.03$  versus  $\Omega_M(WMAP) = 0.27 \pm 0.04$  (Bennett et al. 2003). Because the analysis that leads to the mass–temperature relation we use to estimate our cluster virial masses is so different from the X-ray imaging analysis required to estimate the ICM masses, the agreement between our baryon fraction estimate of  $\Omega_M$  and the *WMAP* estimate suggests that our cluster virial masses and ICM masses must be fairly accurate. In that case we can use the baryon fraction  $\Omega_M$  estimate to constrain differences between the universal and the cluster mass–to–light ratio. Specifically, with the universal mass–to–light ratio  $\Upsilon_{univ} = \Omega_M \rho_c / \bar{j}$  where  $\Omega_M$  is given by cluster baryon fraction, we have  $\Upsilon_{univ} = (78 \pm 13) h_{70}$ , whereas our hot cluster mass–to–light ratio is  $\bar{\Upsilon}_{500,hot} = (53 \pm 3) h_{70}$ . Expressed slightly differently, our measurements imply that  $\Upsilon_{univ} / \bar{\Upsilon}_{500,hot} = 1.46 \pm 0.21$ . It is well known that galaxy morphological mix and star formation rates are very different between the fields and the clusters (e.g. Dressler 1984; Lewis et al. 2002); our measurements thus provide an interesting indication of possible differences in the star formation histories and star formation efficiencies in these two dramatically different environments.

## 4. STAR FORMATION AND ENRICHMENT

Combined analyses of NIR and X-ray observations allow us to address several interesting questions concerning the thermodynamic history of baryons in the clusters: the star formation efficiency (§4.1), the mass fractions of stars and ICM (§4.2), and the metal enrichment of the ICM (§4.3). We discuss the implications of our results on it in §4.4.

### 4.1. Variation of the Star Formation Efficiency



TABLE 2  
DERIVED  $\Omega_M$

Method	Sample	$\Omega_M$
mass-to-light	total (27)	$0.17 \pm 0.02$
ratio $\Upsilon_{500}$	massive (19)	$0.19 \pm 0.03$
baryon	MME (13)	$0.30 \pm 0.03$
fraction $f_b$	MME, massive (10)	$0.28 \pm 0.03$

Note. — Numbers in parentheses indicate the number of clusters in each sample/subsample. “massive” denotes clusters more massive than  $2 \times 10^{14} M_\odot$ . All quantities calculated assuming  $h_{70} = 1$ .

Understanding the cosmic star formation history is of fundamental importance in understanding the formation and evolution of galaxies (e.g. Madau et al. 1998; Springel & Hernquist 2003). Here we estimate the total stellar mass fraction for our sample of 27 clusters. This quantity can be regarded as a tracer of the total mass in stars formed in galaxies within the cluster halo over the course of its collapse. The total stellar mass for each cluster is converted from the total  $K$ -band luminosity, using the derived mean stellar mass-to-light ratio (see §2.2.3 & Appendix). Because NIR light is relatively insensitive to the star formation history, our data should provide a robust estimate of the total stellar mass (within galaxies) in the clusters.

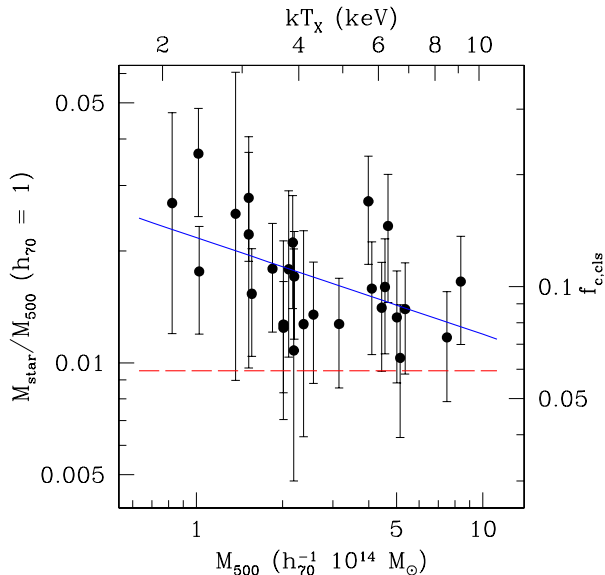


FIG. 7.— Fraction of halo mass that has been turned into stars by the present epoch in our cluster sample. The error budgets are dominated by the uncertainties in the cluster binding mass, which are due to the uncertainties in the X-ray temperature measurement and in the  $M-T_X$  relation (see Table 1). On the right axis is shown the cooled baryon fraction in the clusters (see §4.2 for definition). The dashed line indicates the universal cold baryon fraction (see §4.2).

Figure 7 is a plot of the fraction of the halo mass which is in stars within galaxies for each of our clusters. This fraction varies from  $\sim 2.2\%$  at low mass scales of  $10^{14} h_{70}^{-1} M_\odot$  to  $\sim 1.2\%$  at mass scales of  $10^{15} h_{70}^{-1} M_\odot$ . It is important to note that this fraction does not include any stars that have been stripped from their parent galaxies and are freely orbiting within the galaxy cluster potential, as has

been observed in some cases (Ferguson et al. 1998). Also shown in the figure is the best-fit relation

$$\frac{M_{star}}{M_{500}} = 1.64_{-0.09}^{+0.10} \times 10^{-2} \left( \frac{M_{500}}{3 \times 10^{14} M_\odot} \right)^{-0.26 \pm 0.09} \quad (9)$$

for  $h_{70} = 1$ . Our observations suggest that the integrated star formation efficiency drops by a factor of  $\sim 1.8$  over the mass range of galaxy clusters. Of course, it is also possible that the trend we observe arises because the reservoir of stars that lie outside galaxies is fractionally larger in more massive clusters (e.g. Trentham & Mobasher 1998; Gregg & West 1998).

The decrease in star formation efficiency appears to be broadly consistent with theoretical expectations from state-of-the-art hydrodynamical simulations by Springel & Hernquist (2003). Their model includes radiative cooling and heating of the gas, a multi-phase description of the interstellar medium, a self-regulating star formation mechanism, and the feedback processes from supernova events and galactic outflows. They study star formation within haloes ranging from  $10^8$ – $10^{15} M_\odot$ , and find star formation rates broadly consistent with observations. In their models, the integrated star formation efficiency as a function of halo mass falls by a factor of 5 to 10 over cluster mass scales. The underlying cause is the less efficient formation of cooling flows in halos with virial temperatures above  $10^7$  K (Springel & Hernquist 2003). However, what we observe is the star formation efficiency over all galaxy-mass halos that lie within our cluster halo at the present epoch. Because at early times the star formation efficiency in galaxies will be comparable for those galaxies in low mass and high mass cluster halos, we expect the theoretical prediction for  $M_{star}/M_{500}$  to suggest a much weaker trend. We are currently making a detailed comparison of our observational results with numerical star formation models.

#### 4.2. Variation of the ICM to Stellar Mass Ratio

Another interesting quantity that has received much attention is the ICM to stellar mass ratio,  $M_{ICM}/M_{star}$ , as a function of cluster mass. This quantity can be recast as the cluster cold baryon fraction,  $f_{c,cls} = M_{star}/(M_{star} + M_{ICM}) = (1 + M_{ICM}/M_{star})^{-1}$ , which is relevant in (numerical) studies of cosmic star formation (see Balogh et al. 2001b, and references therein). In this section we examine these quantities for the MME subsample.

Our joint analysis of NIR and X-ray observations shows that  $M_{ICM}/M_{star}$  is an increasing function of cluster mass, varying from a factor of 5.9 for low mass clusters

to a factor of 10.4 for high mass clusters. The best-fit relation for  $h_{70} = 1$  is

$$\frac{M_{ICM}}{M_{star}} = 7.7_{-0.4}^{+0.5} \left( \frac{M_{500}}{3 \times 10^{14} M_{\odot}} \right)^{0.25 \pm 0.07} \quad (10)$$

Over an order of magnitude in mass, there is roughly a two fold increase in  $M_{ICM}/M_{star}$ ; the existence of a trend in these data is significant at the  $3.5\sigma$  level, providing confirmation of the early work by David et al. (1990), who estimated the more massive clusters ( $T_X \sim 7$  keV) have a  $\sim 3\times$  larger  $M_{ICM}/M_{star}$  ratio than do less massive ones ( $T_X \sim 3$  keV). Arnaud et al. (1992) found a correlation between  $M_{ICM}$  and stellar luminosities from early-type galaxies (E+S0); they estimated the mean ICM to stellar mass ratio as 3.6, which is much smaller than the values that we obtain. We note these two early studies evaluated the ICM to stellar mass at different overdensities for different clusters. More recently, Roussel et al. (2000) found no trend when they examined  $M_{ICM}/M_{star}$  at  $r_{200}$  in their combined X-ray and optical sample of 33 clusters and groups. Interestingly, their analysis suggested a trend when measurements were made at  $r_{2000}$ , where less extrapolation of the X-ray data is required.

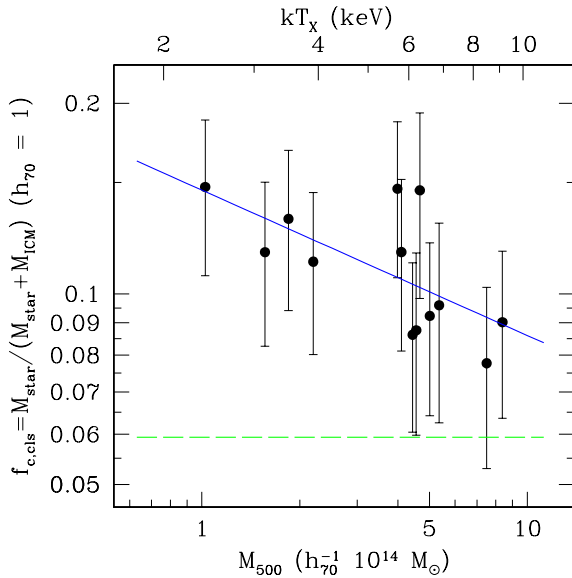


FIG. 8.— The cold baryon fraction of the clusters. This is roughly inversely proportional to the ICM to stellar mass ratio. The solid line is the best-fit to the observed trend. The dashed line shows the universal cold baryon fraction.

In Fig 8 we plot the cluster cold baryon fraction, the ratio of stellar mass to total baryon (star plus ICM) mass. As implied by Eqn 10,  $f_{c,cls}$  is a decreasing function of cluster mass, indicating that the star formation efficiency is smaller in more massive clusters than that in low mass ones. This is in accordance with the conclusion of §4.1; in fact, from the ratio  $M_{star}/M_{500}$  one can infer the cold baryon fraction via  $f_{c,cls} = (M_{star}/M_{500}) \Omega_M / \Omega_b$  (Balogh et al. 2001b), which is shown in the right axis of Fig 7. Also shown in both Figures 7 & 8 (the horizontal dashed line) is the universal cold fraction  $f_{c,univ} = \Omega_{star} / \Omega_b$ , where  $\Omega_{star} = (2.7 \pm 0.3) \times 10^{-3} h_{70}^{-1}$  is obtained by an analysis of 2MASS data (Kochanek et al. 2001). We notice that in both figures the cluster cold fraction approaches the universal value with increasing halo mass.

Our Figures 7 & 8 can be directly compared to the bottom and upper panel of Fig 1 in Balogh et al. (2001b), which was produced using previous observations of 48 clusters and groups (Carlberg et al. 1996; Roussel et al. 2000). In that study, it was argued that the first approach (which utilizes the ratio  $M_{ICM}/M_{star}$ ) produces large scatter for  $f_{c,cls}$ , while the second one (that uses the ratio  $M_{star}/M_{500}$ ) shows a much smaller scatter, and implies cluster cold fractions for all clusters considered are close to the universal value. However, measurements in our sample show this may not be the case. Our results may be more robust, because of the data homogeneity (all NIR photometry based on 2MASS), an improved treatment of stellar mass-to-light ratio, the use of observed X-ray  $M - T$  relation (as opposed to that based on numerical simulations), and the reliability of the ICM mass estimation (all X-ray data extend to  $r_{500}$ ). Studies of a larger sample will provide additional insights into these trends.

### 4.3. ICM Enrichment

Extensive investigations of ICM metal abundances have been carried out (see Arnaud et al. 1992; Renzini 1997 for reviews), but until recently these studies relied on emission-weighted values and were therefore biased toward the abundance at the cluster center. Precision abundance measurement and radial abundance profiles in clusters have only been possible with imaging X-ray observatories such as ASCA, BeppoSax, Chandra and XMM-Newton (e.g. Dupke & White 2000; Finoguenov et al. 2000, 2001a; De Grandi & Molendi 2001, among others).

In the bottom panel of Fig 9, we plot the iron yield, which is the ratio of iron ( $Fe$ ) to stellar mass, as a function of cluster mass in units of solar metallicity:  $y_{cls,Fe} \equiv M_{Fe}/M_{star} = (M_{ICM} Z_{ICM,Fe} + M_{star} Z_{star,Fe})/M_{star}$  (e.g. Arnaud et al. 1992). The ICM iron mass is calculated by assuming the mean mass weighted iron abundance of the ICM to be  $Z_{ICM,Fe} = 0.21 Z_{\odot,Fe}$ , which is deduced from the metallicity profiles in cool core clusters and non-cool core clusters observed by BeppoSax (De Grandi & Molendi 2001, 2003 private communication). For the stellar iron abundance, we account for population trends in the galaxies much as we do in estimating the typical stellar mass-to-light ratio. We assume constant metallicities  $Z_{star,Fe} = 1.2 Z_{\odot,Fe}$  and  $1.8 Z_{\odot,Fe}$  for ellipticals and spirals (Jørgensen 1999; Terlevich & Forbes 2002), respectively, and we weight them by the appropriate stellar mass-to-light ratio, luminosity functions of different morphological types, and the relative abundance of ellipticals and spirals. We detail our approach in the Appendix. The resultant  $Z_{star,Fe}$  is about  $1.45 Z_{\odot,Fe}$  at  $T_X = 2$  keV and about  $1.27 Z_{\odot,Fe}$  at  $T_X = 10$  keV.

The best-fit to the observed trend in our data is

$$y_{cls,Fe} = 2.98_{-0.09}^{+0.10} Z_{\odot,Fe} \left( \frac{M_{500}}{3 \times 10^{14} M_{\odot}} \right)^{0.12 \pm 0.04} \quad (11)$$

for  $h_{70} = 1$ . The iron yield is related to the iron mass-to-light ratio (IMLR, Renzini et al. 1993) which appears frequently in recent literature (e.g. Finoguenov et al. 2000):  $IMLR = y_{cls,Fe} \bar{Y}_{star}$ , where  $\bar{Y}_{star}$  is the mean stellar mass-to-light ratio. Previous studies using blue band optical photometry suggested that IMLR is generally independent of cluster mass (Renzini 1997). The trend in

our sample for increasing  $y_{cls,Fe}$  arises from the increasing ICM mass fraction, an improved understanding of the typical ICM metallicity (De Grandi & Molendi 2001) and the decreasing stellar mass fraction. Fig 9 (lower panel) also shows that the iron yields in the cluster systems are very high relative to the approximately solar metal abundances observed in stars and the interstellar medium in galaxies (Henry & Worthey 1999, and the references therein). It is unlikely that galaxies with a simple star formation history and typical initial mass function (hereafter IMF) could produce such high iron yields (although see Pipino et al. 2002).

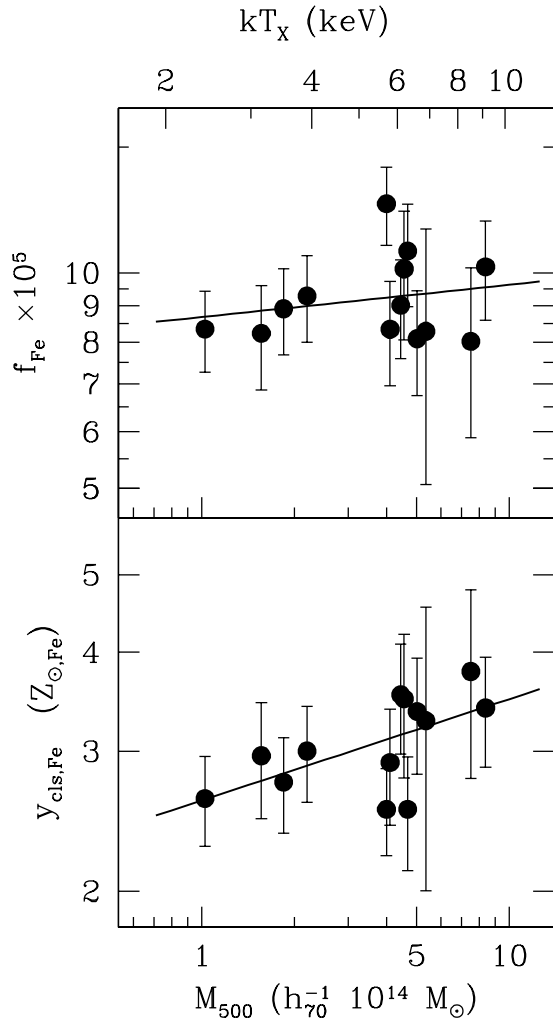


FIG. 9.— The upper panel: the iron mass fraction in the clusters. The lower panel: the iron yield. The ICM iron abundance  $Z_{ICM,Fe} = 0.21 Z_{\odot,Fe}$  from De Grandi & Molendi (2001) is used, and the stellar contribution is calculated by the method stated in the Appendix.

In Fig 9 (upper panel) we plot the iron mass fraction,  $f_{Fe} = M_{Fe}/M_{500}$ , using  $Z_{\odot,Fe} = 1.814 \times 10^{-3}$  (Anders & Grevesse 1989). Unlike the iron yield, which compares the iron mass to the stellar mass in each system, the iron mass fraction shows less apparent trend with respect to the cluster binding mass; the best-fit slope of the iron mass fraction is  $0.048 \pm 0.056$ , consistent with no trend at all. This nearly uniform enrichment of the baryon reservoir in

clusters, combined with the high iron yield and the trend of decreasing star formation efficiency with cluster mass, may suggest that the primary enrichment mechanism in the ICM is not the stars that we observe in the cluster galaxies; instead, the intergalactic gas that becomes the ICM may be pre-enriched by some earlier stellar population that is at work before cluster galaxies form. This process appears to work with similar efficiency over the whole range of cluster masses. One possible mechanism for this uniform enrichment would be population III stars. An early stellar population of massive stars could contribute significantly to the metallicity – both because their likely top-heavy IMF and high metal yields (e.g. Larson 1998; Heger & Woosley 2002) – and presumably enhance the entropy of the gas that eventually collapses to form galaxies and clusters. Another intriguing piece of cluster evidence for population III stars is that the observed elemental abundance ratios in the cluster ICM appear to be difficult to explain by reasonable combinations of Type I and Type II supernovae (Loewenstein 2001).

#### 4.4. Thermodynamic History of the ICM

Clearly the intersection of cluster structure and the cosmic star formation history is an intriguing avenue for further research. The star formation efficiency, the ratio of ICM mass to stellar mass and the total iron mass provide important insights into the thermodynamic history of the ICM. These results, taken together with existing observations of other cluster scaling relations (e.g.  $L_X - T_X$ ,  $M_{ICM} - T_X$ ,  $R_I - T_X$ , where  $R_I$  is the X-ray isophotal size of clusters) provide an abundance of evidence that cluster ICM and stellar properties do not scale self-similarly (e.g. MME, David et al. 1993; Mohr & Evrard 1997; Arnaud & Evrard 1999; Lloyd-Davies et al. 2000). One interpretation has been that the gas distribution in low mass clusters has been altered relative to the expectations of the standard formation scenario by the addition of entropy or “preheating” by galaxy formation at early times (Kaiser 1991; Evrard & Henry 1991; Cavaliere et al. 1997; Wu et al. 2000; Bialek et al. 2001; Muanwong et al. 2002). In this picture, prior to the cluster/group collapse, the intergalactic gas is heated by, e.g., supernova-driven galactic outflows or AGN. The preheated, high-entropy gas thus forms a more extended distribution when it collapses into the cluster scale halos. The effect is less prominent in more massive systems, because in these massive systems the entropy increase in the ICM due to strong accretion shocks is much larger than that caused by preheating. This framework provides a means of explaining the observed slopes of the  $M_{ICM} - T_X$ ,  $L_X - T_X$  and  $R_I - T_X$  relations, if preheating enhances the entropy by about  $\sim 100 \text{ keV cm}^2$  (Bialek et al. 2001). This level of preheating appears to be consistent with the cluster “entropy floor” observed by Lloyd-Davies et al. (2000).

Despite the successes of the preheating model in explaining observed cluster ICM properties, a generic problem with this model is the large energy required if carried out in the dense ICM in the centers of clusters or in the early universe (e.g. Bryan 2000; Wu et al. 2000). To circumvent these difficulties, Bryan (2000) proposed an alternative to the preheating model in which the star formation efficiency varies as a function of halo mass. The gas that cools to

TABLE 3  
SCALING RELATIONS

Quantity	Normalization	Slope
X	a	b
$L_{500}$	$3.0^{+0.4}_{-0.3} 10^{12} L_{\odot}$	$0.63 \pm 0.09$
$\Upsilon_{500}$	$32 \pm 4 \Upsilon_{\odot}$	$0.31 \pm 0.09$
$f_b$	$0.13 \pm 0.08$	$0.15 \pm 0.04$
$f_{star}$	$0.022^{+0.003}_{-0.002}$	$-0.26 \pm 0.09$
$M_{ICM}/M_{star}$	$5.9^{+0.8}_{-0.7}$	$0.30 \pm 0.07$
$y_{Fe}$	$2.6 \pm 0.2 Z_{\odot, Fe}$	$0.12 \pm 0.04$

Note. — Scaling relations in the form of  $X = a (M_{500}/10^{14} M_{\odot})^b$ . Uncertainties at  $1\sigma$  level. All quantities calculated assuming  $h_{70} = 1$ .

form stars is the lowest entropy gas, and its removal from the cluster causes similar structural signatures to those produced in the preheating scenario (see also Voit et al. 2002; Muanwong et al. 2002; Nath 2002).

The NIR and X-ray properties of our cluster ensemble appear to provide problems for both the preheating and star formation efficiency scenarios. Namely, the direct evidence for a decreasing star formation efficiency with increasing cluster mass (Fig 7) lies outside the bounds of simple preheating scenarios, and the increasing total baryon fraction is at odds with simple models where the total baryon fraction is constant in clusters but the fraction cooling into stars is changing. Moreover, the high metallicity of the ICM together with the large ICM mass to stellar mass ratio strongly suggests that the source of enrichment (and so perhaps the entropy as well) requires something more than star formation with a typical initial mass function. It appears likely that more complex models that include both varying star formation efficiency, preheating and enrichment at early times are necessary to explain these observations.

## 5. SYSTEMATIC UNCERTAINTIES

There are several key ingredients of our analysis: the cluster sample selection, the X-ray  $M - T_X$  relation, the ICM mass measurement, the total NIR luminosity, the mean NIR stellar mass-to-light ratio, and the ICM and stellar metallicities. These affect the derived NIR luminosity, the stellar mass fraction, the cluster baryon fraction, and the iron mass fraction, as a function of cluster mass. In what follows we discuss the robustness of these ingredients.

*Cluster sample selection:* Our cluster sample is taken partly from an X-ray flux limited sample and partly from a medley of clusters with available X-ray temperature measurements. Our results may depend on this selection, because low mass clusters in our sample tend to be at lower redshift than the higher mass clusters. Any redshift related systematic could then potentially masquerade as a mass trend. We examine this possibility in Fig 2, where we compare the luminosity function parameters for different mass and redshift ranges. As discussed in §2.2.2, after dividing the sample into two mass subsamples, we find no redshift trends in luminosity function parameters.

*$M - T_X$  relation:* The  $M - T_X$  determines the cluster mass and the virial radius. We adopt the observed rela-

tion based on ASCA measurements of cluster temperature profiles (Finoguenov et al. 2001b). The self-similar cluster evolution scenario predicts the slope to be 1.5, which is consistent with the observed value we use. Using a slope of 1.5 (with a normalization chosen to be the same as the observed one at  $T_X = 6$  keV) produces best-fit relations that are statistically consistent with the fiducial results. However, we notice that shifts in normalization can be important – in most of the cases crucial – to estimates of the cluster baryon fraction, mass-to-light ratio, and stellar mass fraction; however, normalization uncertainties do not affect the trends we see with cluster virial mass.

*ICM mass:* All our ICM masses are from ROSAT PSPC X-ray surface brightness profiles that extend to or near  $r_{500}$ , based on the adopted  $M - T_X$  relation. We also take into account the clumping in the ICM and depletion of the baryon fraction at  $r_{500}$  using results from hydrodynamical simulations (MME).

*NIR luminosity:* We use the second release data from 2MASS, which has accurate photometry and a small star-galaxy misidentification rate. Major factors that affect the estimates of the total NIR luminosity include: the cluster angular size (mainly by  $T_X$  &  $M - T_X$  relation), the faint-end slope  $\alpha$  of the luminosity function, the contributions from the BCGs, and the method of background subtraction. In the case that mass and light have the same distribution, whether we choose  $r_{500}$  or  $r_{200}$  should not affect our results. Currently we are restricted by the sky coverage of 2MASS second release data: we have NIR data only out to  $r_{500}$  for some of the clusters, which increases the uncertainties in estimating light at  $r_{200}$ . We have examined the light-mass relation at  $r_{200}$ , and the best-fit slope is statistically consistent with that at  $r_{500}$ . The faint-end slope of the luminosity function  $\alpha$  has very little effect for those nearby clusters that 2MASS has probed deeply enough to measure a large fraction of light, but for clusters with larger redshifts, the effects are larger. Overall, though, the best-fit slopes calculated for several different values of  $\alpha$  are consistent with the fiducial ones. Finally, the statistical and “annulus” methods for background subtraction give statistically consistent results. It is interesting to notice that, based on the observed  $K$ -band  $\log N - \log S$  relation, the probability that a foreground galaxy 2 magnitudes brighter than  $M_*$  lies within the cluster region increases slightly with redshift for our sample; light from a chance superposition like this is subtracted statistically.

However, if there were any residual bias, the effect would be to add more light to higher redshift (which tend to be more massive) clusters, which would weaken the trend in mass-to-light ratio that we observe.

*Mean stellar mass-to-light ratio:* We use this to estimate the stellar mass and the associated quantities. Instead of using a varying mass-to-light ratio based on the (somewhat uncertain) spiral fraction and the (also uncertain) stellar mass-to-light ratio in elliptical and spiral galaxies, we could assume a constant mass-to-light ratio given by 2dF survey (Cole et al. 2001, see §2.2.3). Using this constant mass-to-light ratio gives scaling relations that have slopes about  $0.5 - 1\sigma$  different from our fiducial ones.

*Mean ICM  $\mathcal{E}$  stellar metallicities:* These quantities are used to convert stellar and ICM mass into iron mass. The ICM iron abundance is measured to be relatively constant against  $T_X$  (De Grandi 2003, private communication), and the value that we adopt is representative of the ICM as a whole. The stellar iron abundance, on the other hand, suffers difficulties that are similar to the mean stellar mass-to-light ratio, due to uncertainties in observations and the relative spiral and elliptical abundance. If we assume solar abundance for stars in all galaxies, we obtain a  $y_{Fe} - M$  relation with slope  $\sim 1.5\sigma$  steeper than the fiducial one.

In summary, as far as the best-fit results are concerned, all the effects considered above give consistent results with our fiducial results; the factors that give largest deviations are the faint-end slope of the luminosity function and the choice of cluster region. Other factors, such as the assumed cosmology in calculating the distance to the clusters, or the Malmquist bias (less than 3%), do not affect our results. We therefore conclude that the results presented in the previous sections are robust. We look forward to better examining sample selection issues once the full 2MASS dataset is available.

## 6. SUMMARY & PROSPECTS

We have used the NIR data from the 2MASS survey together with archival and published X-ray data to analyze the properties of the stellar and ICM baryon reservoirs in galaxy clusters. While X-ray temperature gives us reliable cluster binding mass estimates, NIR light traces stellar population better than optical bands; the joint analysis makes it possible to examine whether stellar NIR luminosity can serve as a good cluster mass estimator. It also enables us to probe the star formation efficiency for clusters spanning an order of magnitude in mass. For a subsample of 13 clusters, we also measure ICM masses from X-ray data. We are therefore able to investigate the relative abundance of the main baryonic components in clusters, as well as the issues concerning the ICM iron enrichment processes. We review our conclusions here, and summarize the scaling relations in Table 3.

First, the NIR properties of galaxy clusters appear to exhibit significant regularity. The  $K$ -band luminosity within  $r_{500}$  is strongly correlated with the cluster binding mass, with an observed scatter of approximately 28% in  $K$ -band luminosity at a fixed cluster mass. Thus, the NIR cluster light is a good predictor of cluster mass. The  $K$ -band mass-to-light ratio increases from  $\Upsilon_{500} \sim 33 h_{70} \Upsilon_{\odot}$  for  $10^{14} h_{70}^{-1} M_{\odot}$  clusters to  $\Upsilon_{500} \sim 68 h_{70} \Upsilon_{\odot}$  for  $10^{15} h_{70}^{-1} M_{\odot}$

clusters. This trend must be accounted for when interpreting NIR cluster surveys, where the NIR light is the primary indicator of cluster mass. However, we also notice that for clusters more massive than  $2 \times 10^{14} h_{70}^{-1} M_{\odot}$  ( $T_X \geq 3.7$  keV) there is little evidence for a changing mass-to-light ratio.

Second, the cluster baryon fraction together with constraints from the CMB observations on  $\Omega_b$  provides a measure of the matter density parameter  $\Omega_M = 0.28 \pm 0.03$  (for  $h_{70} = 1$ ) that is in excellent agreement with recent CMB anisotropy results.

Third, the mass-to-light ratio of the most massive clusters can be used with a measure of the  $K$ -band luminosity density of the universe to estimate the matter density parameter  $\Omega_M = 0.19 \pm 0.03$ . Alternatively, adopting the baryon fraction constraint on  $\Omega_M$ , we show that the  $K$ -band mass-to-light ratio in the universe must be  $\bar{\Upsilon}_{univ} = (78 \pm 13) h_{70} \Upsilon_{\odot}$ . This mass-to-light ratio is marginally consistent with that for our more massive clusters  $\bar{\Upsilon}_{500,hot} = (53 \pm 3) h_{70} \Upsilon_{\odot}$ , indicating that differences in the star formation history in these environments produce present epoch mass-to-light ratios that differ by as much as  $\sim 30\%$ .

Fourth, the amount of  $K$ -band light per unit cluster binding mass is a factor of  $\sim 2$  times higher for low mass clusters than for high mass clusters. Accounting for a slight variation in the mean  $K$ -band stellar mass-to-light ratio for galaxies in low and high mass clusters, we find that the overall star formation efficiency decreases with increasing cluster mass. This observation provides a new constraint on developing galaxy formation models.

Fifth, the decreasing stellar mass fraction and increasing ICM mass fraction lead to a ratio of ICM mass to stellar mass that varies from 5.9 to 10.4 over the cluster mass range of  $10^{14} h_{70}^{-1} M_{\odot}$  to  $10^{15} h_{70}^{-1} M_{\odot}$ . Thus, stars constitute roughly 14% of the baryons in low mass clusters and only 9% in high mass clusters.

Sixth, the trends in stellar mass and ICM mass with cluster binding mass provide useful constraints on the thermodynamic history of galaxy clusters. Specifically, pure preheating models are inconsistent with our observations, because preheating of the ICM would not introduce a decreasing star formation efficiency. In addition, simple cooling-oriented models that suggest a constant baryon fraction with a larger portion of the baryons going into stars in low mass clusters are inconsistent with our observations, because the total baryon fraction is increasing with cluster mass in our sample. Models that include varying star formation efficiency *and* preheating or cooling to achieve a minimum entropy level in the ICM of  $\sim 100$  keV  $\text{cm}^2$  would likely reproduce the observed trends.

Seventh, the iron yield per unit stellar mass is large and an increasing function of cluster binding mass. It is likely that unusually top-heavy stellar initial mass functions would be required to enrich the baryons to such a high level. Interestingly, the iron fraction (ratio of iron mass to cluster binding mass) is roughly constant. Together with the trend of decreasing stellar mass fraction, this constant iron mass fraction suggests that there may have been an early epoch of star formation and enrichment – perhaps before the epoch of galaxy formation –

that acted uniformly over the full range of cluster masses.

Due to the incomplete sky coverage of the 2MASS second incremental release, our analysis is restricted to a small sample of 27 clusters; the shallow 2MASS photometry limits our study to low redshift clusters. We plan to expand the analysis presented here to a much larger sample of local clusters, as well as to clusters at higher redshift using deeper photometry. Together, these studies will lead us toward a more complete understanding of the evolution of galaxy clusters and their baryon reservoirs. This understanding will undoubtedly contribute to interesting cosmological studies and an improved understanding of the star formation history of the universe.

We thank an anonymous referee for comments that improved the paper. We extend our thanks to Chris Kochanek, Martin White, Thomas Reiprich and Anthony

Gonzalez for helpful comments on an early version of the manuscript. YTL thanks Subha Majumdar, Al Sanderson and I.H. for helpful discussions. JJM acknowledges financial support from the NASA Long Term Space Astrophysics grant NAG 5-11415. SAS acknowledges financial support from the NASA Long Term Space Astrophysics grant NAG 5-8430. This publication makes use of data products from the Two Micron All Sky Survey, which is a joint project of the University of Massachusetts and the Infrared Processing and Analysis Center, funded by the National Aeronautics and Space Administration and the National Science Foundation. This research has made use of the NASA/IPAC Extragalactic Database (NED) which is operated by the Jet Propulsion Laboratory, California Institute of Technology, under contract with the National Aeronautics and Space Administration.

## APPENDIX

Here we describe our estimate of the mean stellar mass-to-light ratio for each cluster. As a simplified model, we divide galaxies into early and late types and calculate the average stellar mass-to-light ratio in the two types. We employ published estimates of the stellar mass-to-light ratio as a function of mass and luminosity in both ellipticals and spirals. With published estimates of the spiral fraction as a function of cluster mass and of the luminosity function for ellipticals and spirals, we then calculate the luminosity-weighted mean stellar mass-to-light ratio. We describe each of these steps in turn.

For the  $K$ -band stellar mass-to-light ratio in ellipticals, we use the results of a dynamical analysis of 21 luminous ellipticals (Gerhard et al. 2001). Specifically, from their Fig 13 we estimate the central mass-to-light ratio  $\Upsilon_e(L)$  as a function of galaxy luminosity, using the typical color for ellipticals  $B - K \approx 4.1$  (Pahre 1999). The central mass-to-light ratio is a good estimate of the stellar mass-to-light ratio, because the central regions of ellipticals are dominated by stellar mass. For the  $K$ -band stellar mass-to-light ratio of spiral galaxies, we use the results of Bell & de Jong (2001, see their Fig 1), who construct models that describe many characteristics of spirals in the Ursa Major cluster.

We adopt the  $K$ -band luminosity functions (characterized by the Schechter parameters  $\alpha$  and  $L_*$ ) from a  $K$ -band 2MASS study (Kochanek et al. 2001). With subscripts  $e$  &  $s$  denoting “elliptical” & “spiral”, respectively, the mean stellar mass-to-light ratio is

$$\bar{\Upsilon}_{star} = \frac{n_e L_{*,e} \int_{y_{low,e}}^{\infty} \Upsilon_e(y) e^{-y} y^{\alpha_e+1} dy + n_s L_{*,s} \int_{y_{low,s}}^{\infty} \Upsilon_s(y) e^{-y} y^{\alpha_s+1} dy}{n_e L_{*,e} \int_{y_{low,e}}^{\infty} e^{-y} y^{\alpha_e+1} dy + n_s L_{*,s} \int_{y_{low,s}}^{\infty} e^{-y} y^{\alpha_s+1} dy},$$

where  $y_{low,i} \equiv L_{low}/L_{*,i}$  ( $i = e, s$ ),  $L_{low}$  corresponds to  $M_{low} = -20$ , the luminosity cutoff (see §2.2.3), the galaxy number densities  $n_e$  &  $n_s$  are determined from the total number of galaxies observed  $n'_{tot} = \int_{L_{low}/L_*}^{\infty} \phi_*(L/L_*)^\alpha \exp(-L/L_*) d(L/L_*)$  and the spiral galaxy number fraction  $f_s$ :  $n_e = n'_{tot}(1 - f_s) / \int_{y_{low,e}}^{\infty} e^{-y} y^{\alpha_e} dy$ ,  $n_s = n'_{tot} f_s / \int_{y_{low,s}}^{\infty} e^{-y} y^{\alpha_s} dy$ . As explained earlier, the integration limits are chosen to avoid integrating over the faint-end of the luminosity functions whose shape is unknown and where the behavior of galaxy  $\Upsilon(L)$  is also unknown.

We use early published estimates of the spiral fraction to measure the trend in  $f_s$  with cluster  $T_X$  (Bahcall 1977b; Dressler 1980; Dressler & Shectman 1988). For the 28 clusters from these data sets with published  $T_X$ , we regard all galaxies designated as cD, E and S0 as ellipticals, and we ignore irregulars. The resulting spiral fraction decreases with cluster temperature. The best-fit to the  $f_s - T_X$  relation is  $\log f_s = -0.5 \log(T_X/4\text{keV}) - 0.4$ . For each cluster in our sample we calculate  $f_s(T_X)$ , then use the above expression to calculate the mean stellar mass-to-light ratio. The resulting  $\bar{\Upsilon}_{star}$  varies weakly with  $T_X$  (from  $\sim 0.7\Upsilon_\odot$  at 2 keV to  $\sim 0.8\Upsilon_\odot$  at 10 keV). Curiously, the value at low mass end is very close to that obtained by Cole et al. (2001), using a Kennicutt (1983) IMF (see Fig 3).

Let us point out some caveats for the above approach. First of all, the galaxy mass-to-light ratios are not solely from observations of cluster galaxies (elliptical mass-to-light ratio are observed but not for galaxies in clusters; spiral mass-to-light ratio are from models built from observations of cluster galaxies, see above), and the luminosity functions used to calculate the mean mass-to-light ratio are based on all the galaxies with  $cz > 2500 \text{ km s}^{-1}$ , which includes both cluster and field galaxies (Kochanek et al. 2001). We simply assume that these “field” luminosity functions are applicable to cluster environments. Finally, the spiral abundances presented in Bahcall (1977b) and Dressler (1980) are based on visual/blue band observations (which may be larger than the values obtained when observed at redder bands), and are not restricted to a fixed fraction of virial radius or a fraction of the luminosity function comparable to that we use in our 2MASS study; thus, the uncertainty in  $f_s$  is therefore probably significant and should be examined directly in the 2MASS data.

Following a similar line of reasoning, we calculate the mean stellar metallicity based on the observed iron abundance

for stars in elliptical and spiral galaxies  $Z_e$  &  $Z_s$ :

$$\bar{Z}_{star,Fe} = \frac{n_e L_{*,e} \int_{y_{low,e}}^{\infty} Z_e(y) \Upsilon_e(y) e^{-y} y^{\alpha_e+1} dy + n_s L_{*,s} \int_{y_{low,s}}^{\infty} Z_s(y) \Upsilon_s(y) e^{-y} y^{\alpha_s+1} dy}{n_e L_{*,e} \int_{y_{low,e}}^{\infty} \Upsilon_e(y) e^{-y} y^{\alpha_e+1} dy + n_s L_{*,s} \int_{y_{low,s}}^{\infty} \Upsilon_s(y) e^{-y} y^{\alpha_s+1} dy}.$$

For stellar iron abundance in ellipticals we use the results from a study of 115 E/S0 galaxies in Coma (Jørgensen 1999). This analysis showed that there is no clear correlation between  $[Fe/H]$  and galaxy mass or luminosity. The median value of  $[Fe/H]$  is  $\sim 0.1$ , which corresponds to  $Z_e \sim 1.2Z_{\odot,Fe}$ . For spiral metallicity, we examine measurements for 14 spirals in cluster/group environments (Terlevich & Forbes 2002).  $[Fe/H]$  of these spirals does not show a clear correlation with galaxy luminosity; the mean  $[Fe/H] \sim 0.25$ , or  $Z_s \sim 1.8Z_{\odot,Fe}$ . Assuming these metallicities are representative for all spirals and ellipticals, the resultant mean metallicity  $\bar{Z}_{star,Fe}$  is about 1.45 at  $T_X = 2$  keV and about 1.27 at  $T_X = 10$  keV.

## REFERENCES

- Allen, S. W., Schmidt, R. W., & Fabian, A. C. 2002, MNRAS, 334, L11
- Anders, E. & Grevesse, N. 1989, Geochim. Cosmochim. Acta, 53, 197
- Andreon, S. & Pelló, R. 2000, A&A, 353, 479
- Arnaud, M. & Evrard, A. E. 1999, MNRAS, 305, 631
- Arnaud, M., Rothenflug, R., Boulade, O., Vigroux, L., & Vangioni-Flam, E. 1992, A&A, 254, 49
- Bahcall, N. A. 1977a, ARA&A, 15, 505
- . 1977b, ApJ, 218, L93
- Bahcall, N. A. & Comerford, J. M. 2002, ApJ, 565, L5
- Bahcall, N. A., Lubin, L. M., & Dorman, V. 1995, ApJ, 447, L81
- Bahcall, N. A. & Soneira, R. M. 1983, ApJ, 270, 20
- Balogh, M. L., Christlein, D., Zabludoff, A. I., & Zaritsky, D. 2001a, ApJ, 557, 117
- Balogh, M. L., Pearce, F. R., Bower, R. G., & Kay, S. T. 2001b, MNRAS, 326, 1228
- Bell, E. F. & de Jong, R. S. 2001, ApJ, 550, 212
- Bennett, C. L., Halpern, M., Hinshaw, G., Jarosik, N., Kogut, A., Limon, M., Meyer, S. S., Page, L., Spergel, D. N., Tucker, G. S., Wollack, E., Wright, E. L., Barnes, C., Greason, M. R., Hill, R. S., Komatsu, E., Nolte, M. R., Odegard, N., Peirs, H. V., Verde, L., & Weiland, J. L. 2003, ApJ, submitted (astro-ph/0302207)
- Bialek, J. J., Evrard, A. E., & Mohr, J. J. 2001, ApJ, 555, 597
- Bruzual A., G. & Charlot, S. 1993, ApJ, 405, 538
- Bryan, G. L. 2000, ApJ, 544, L1
- Carlberg, R. G., Yee, H. K. C., Ellingson, E., Abraham, R., Gravel, P., Morris, S., & Pritchet, C. J. 1996, ApJ, 462, 32
- Cavaliere, A., Menci, N., & Tozzi, P. 1997, ApJ, 484, L21
- Cole et al. 2001, MNRAS, 326, 255
- David, L. P., Arnaud, K. A., Forman, W., & Jones, C. 1990, ApJ, 356, 32
- David, L. P., Jones, C., & Forman, W. 1995, ApJ, 445, 578
- David, L. P., Slyz, A., Jones, C., Forman, W., Vrtilik, S. D., & Arnaud, K. A. 1993, ApJ, 412, 479
- De Grandi, S. & Molendi, S. 2001, ApJ, 551, 153
- De Propriis, R., Colless, M., Driver, S., Couch, W., Peacock, J., Baldry, I., Baugh, C., Collins, C., Bland-Hawthorn, J., Bridges, T., Cannon, R., Cole, S., Cross, N., Dalton, G. B., Efstathiou, G., Ellis, R. S., Frenk, C. S., Glazebrook, K., Hawkins, E., Jackson, C., Lahav, O., Lewis, I., Lumsden, S., Maddox, S., Madgwick, D. S., Norberg, P., Percival, W., Peterson, B., Sutherland, W., & Taylor, K. 2002, MNRAS, submitted (astro-ph/0212562)
- Dressler, A. 1980, ApJS, 42, 565
- . 1984, ARA&A, 22, 185
- Dressler, A. & Shectman, S. A. 1988, AJ, 95, 284
- Dupke, R. A. & White, R. E. 2000, ApJ, 537, 123
- Edge, A. C. & Stewart, G. C. 1991, MNRAS, 252, 414
- Ettori, S. & Fabian, A. C. 1999, MNRAS, 305, 834
- Evrard, A. E. 1997, MNRAS, 292, 289
- Evrard, A. E. & Henry, J. P. 1991, ApJ, 383, 95
- Ferguson, H. C., Tanvir, N. R., & von Hippel, T. 1998, Nature, 391, 461
- Finoguenov, A., Arnaud, M., & David, L. P. 2001a, ApJ, 555, 191
- Finoguenov, A., David, L. P., & Ponman, T. J. 2000, ApJ, 544, 188
- Finoguenov, A., Reiprich, T. H., & Böhringer, H. 2001b, A&A, 368, 749
- Gavazzi, G., Pierini, D., & Boselli, A. 1996, A&A, 312, 397
- Gerhard, O., Kronawitter, A., Saglia, R. P., & Bender, R. 2001, AJ, 121, 1936
- Girardi, M., Borgani, S., Giuricin, G., Mardirossian, F., & Mezzetti, M. 2000, ApJ, 530, 62
- Girardi, M., Manzato, P., Mezzetti, M., Giuricin, G., & Limboz, F. 2002, ApJ, 569, 720
- Gregg, M. D. & West, M. J. 1998, Nature, 396, 549
- Grego, L., Carlstrom, J. E., Reese, E. D., Holder, G. P., Holzappel, W. L., Joy, M. K., Mohr, J. J., & Patel, S. 2001, ApJ, 552, 2
- Haiman, Z. ., Mohr, J. J., & Holder, G. P. 2001, ApJ, 553, 545
- Heger, A. & Woosley, S. E. 2002, ApJ, 567, 532
- Henry, R. B. C. & Worthey, G. 1999, PASP, 111, 919
- Holder, G., Haiman, Z. ., & Mohr, J. J. 2001, ApJ, 560, L111
- Hradecky, V., Jones, C., Donnelly, R. H., Djorgovski, S. G., Gal, R. R., & Odewahn, S. C. 2000, ApJ, 543, 521
- Jørgensen, I. 1999, MNRAS, 306, 607
- Kaiser, N. 1991, ApJ, 383, 104
- Kennicutt, R. C. 1983, ApJ, 272, 54
- Kochanek, C. S., Pahre, M. A., Falco, E. E., Huchra, J. P., Mader, J., Jarrett, T. H., Chester, T., Cutri, R., & Schneider, S. E. 2001, ApJ, 560, 566
- Kochanek, C. S., White, M., Huchra, J., Macri, L., Jarrett, T. H., Schneider, S. E., & Mader, J. 2002, ApJ, submitted (astro-ph/0208168)
- Larson, R. B. 1998, MNRAS, 301, 569
- Levine, E. S., Schulz, A. E., & White, M. 2002, ApJ, submitted (astro-ph/0204273)
- Lewis, I., Balogh, M., De Propriis, R., Couch, W., Bower, R., Offer, A., Bland-Hawthorn, J., Baldry, I. K., Baugh, C., Bridges, T., Cannon, R., Cole, S., Colless, M., Collins, C., Cross, N., Dalton, G., Driver, S. P., Efstathiou, G., Ellis, R. S., Frenk, C. S., Glazebrook, K., Hawkins, E., Jackson, C., Lahav, O., Lumsden, S., Maddox, S., Madgwick, D., Norberg, P., Peacock, J. A., Percival, W., Peterson, B. A., Sutherland, W., & Taylor, K. 2002, MNRAS, 334, 673
- Lloyd-Davies, E. J., Ponman, T. J., & Cannon, D. B. 2000, MNRAS, 315, 689
- Loewenstein, M. 2001, ApJ, 557, 573
- Madau, P., Pozzetti, L., & Dickinson, M. 1998, ApJ, 498, 106
- Majumdar, S. & Mohr, J. J. 2002, ApJ, accepted (astro-ph/0208002)
- Mathiesen, B., Evrard, A. E., & Mohr, J. J. 1999, ApJ, 520, L21
- Miller, C. J. & Batuski, D. J. 2001, ApJ, 551, 635
- Mobasher, B. & Trentham, N. 1998, MNRAS, 293, 315
- Mohr, J. J. & Evrard, A. E. 1997, ApJ, 491, 38
- Mohr, J. J., Mathiesen, B., & Evrard, A. E. 1999, ApJ, 517, 627
- Muanwong, O., Thomas, P. A., Kay, S. T., & Pearce, F. R. 2002, MNRAS, 336, 527
- Nath, B. B. 2002, MNRAS, accepted (astro-ph/0210410)
- Navarro, J. F., Frenk, C. S., & White, S. D. M. 1997, ApJ, 490, 493
- Pahre, M. A. 1999, ApJS, 124, 127
- Pahre, M. A., de Carvalho, R. R., & Djorgovski, S. G. 1998, AJ, 116, 1606
- Pipino, A., Matteucci, F., Borgani, S., & Biviano, A. 2002, New Astronomy, 7, 227
- Reiprich, T. H. & Böhringer, H. 2002, ApJ, 567, 716
- Renzini, A. 1997, ApJ, 488, 35
- Renzini, A., Ciotti, L., D'Ercole, A., & Pellegrini, S. 1993, ApJ, 419, 52
- Rines, K., Geller, M. J., Kurtz, M. J., Diaferio, A., Jarrett, T. H., & Huchra, J. P. 2001, ApJ, 561, L41
- Roussel, H., Sadat, R., & Blanchard, A. 2000, A&A, 361, 429
- Schechter, P. 1976, ApJ, 203, 297
- Schuecker, P., Guzzo, L., Collins, C. A., & Böhringer, H. 2002, MNRAS, 335, 807
- Springel, V. & Hernquist, L. 2003, MNRAS, 339, 312
- Sunyaev, R. A. & Zel'dovich, Y. B. 1970, Ap&SS, 7, 3
- . 1972, Comments Astrophys. Space Phys., 4, 173
- Terlevich, A. I. & Forbes, D. A. 2002, MNRAS, 330, 547
- Trentham, N. & Mobasher, B. 1998, MNRAS, 293, 53
- Trimble, V. 1987, ARA&A, 25, 425
- Tustin, A. W., Geller, M. J., Kenyon, S. J., & Diaferio, A. 2001, AJ, 122, 1289

- Viana, P. T. P. & Liddle, A. R. 1999, MNRAS, 303, 535  
Voit, G. M., Bryan, G. L., Balogh, M. L., & Bower, R. G. 2002, ApJ, 576, 601  
Wang, L. & Steinhardt, P. J. 1998, ApJ, 508, 483  
White, D. A. 2000, MNRAS, 312, 663  
White, D. A. & Fabian, A. C. 1995, MNRAS, 273, 72  
White, S. D. M., Efstathiou, G., & Frenk, C. S. 1993a, MNRAS, 262, 1023  
White, S. D. M., Navarro, J. F., Evrard, A. E., & Frenk, C. S. 1993b, Nature, 366, 429  
Wu, K. K. S., Fabian, A. C., & Nulsen, P. E. J. 2000, MNRAS, 318, 889